Physics – Uspekhi **67** (5) 487 – 509 (2024)

REVIEW OF TOPICAL PROBLEMS

PACS numbers: 07.07.Df, 87.19.xv, 87.85.fk

Wearable noninvasive glucose sensors based on graphene and other carbon materials

I V Antonova, A I Ivanov

DOI: https://doi.org/10.3367/UFNe.2023.08.039541

Contents

Abstract. Diabetes is one of the most prevalent and chronic diseases worldwide and one of the fastest growing global health emergencies of the 21st century. Since diabetes is a multisystem disease that requires complex treatment, regular analysis of the health condition of patients with diabetes is necessary. With the development of wearable medical systems for monitoring human health, there is a huge potential for testing and, as a result, improving diabetes treatment. The purpose of the present review is to evaluate current developments in wearable biosensors for type 2 diabetes for personalized medicine. In particular, we will consider possibilities of sweat testing for noninvasive analysis of glucose levels in sweat and, consequently, in blood. Wearable biosensors, as a convenient means of measurement, have become a rapidly growing area of interest due to their ability to integrate traditional medical diagnostic tools with miniature laboratory-on-body analytical devices. Diabetes is best treated through tight glycemic control by monitoring glucose levels. The availability of regular testing for an individual's condition is of great importance. Recently, various methods for sensory analysis of diabetes biomarkers have been developed based on new principles, in particular, using various carbon materials (carbon dots, graphene, and carbon tubes). These methods are discussed in this review.

I V Antonova [(1, 2, *)], **A I Ivanov** [(1, **)]
[(1)] Rzhanov Institute of Semiconductor Physics,
Siberian Branch of Russian Academy of Sciences,
prosp. Lavrent'eva 13, 630090 Novosibirsk, Russian Federation
[(2)] Novosibirsk State Technical University,
prosp. Karla Marksa 20, 630087 Novosibirsk, Russian Federation
E-mail: [(*)] antonova@isp.nsc.ru, [(**)] ivanov@isp.nsc.ru

Received 28 March 2023, revised 7 August 2023
Uspekhi Fizicheskikh Nauk **194** (5) 520 – 545 (2024)
Translated by I A Ulitkin

Keywords: wearable biosensors, glucose, principles of analysis, achievements, technologies for the development of sensors, current response, sensitivity

1. Introduction

Diabetes is a chronic disease and one of the fastest growing global health emergencies of the 21st century. According to the International Diabetes Federation (IDF), global diabetes prevalence in 2019 was estimated to be 463 million people, rising to 573 million people in 2021 (10.5% of the global population at the time). By 2030 and 2045, IDF projections show that the number will reach 643 million and 783 million, respectively (Figs 1 and 2) [1]. This circumstance makes glucose monitoring relevant and extremely important, as a result of which a huge amount of diverse research and development is happening [2–4]. The debate about the correlation between glucose levels in alternative biological fluids (for example, tears, saliva, sweat) and blood remains open and topical [5]. In addition, the availability of biosensors and their efficiency is an important factor for their application. The development of existing and novel approaches to noninvasive biofluid-based glucose monitoring, the reliability of which is comparable to that of blood testing, provides a particularly attractive prospect for patients using daily glucose monitoring, i.e., an important part of the diabetes treatment process in the future.

The concept of a glucose sensor was first proposed in 1962 by Clark and Lyons [6], who described an amperometric electrode for determining blood glucose through an enzymatic method, using glucose oxidase (GOx). The GOx enzyme catalyzes the oxidation of glucose, leading to the formation of hydrogen peroxide, the concentration of which is proportional to that of glucose [2, 7–9], as shown in equation of the chemical reaction (1):

$$\text{Glucose} + \text{H}_2 + \text{H}_2\text{O} \xrightarrow{\text{GOx}} \text{gluconic acid} + \text{H}_2\text{O}_2\,. \qquad (1)$$

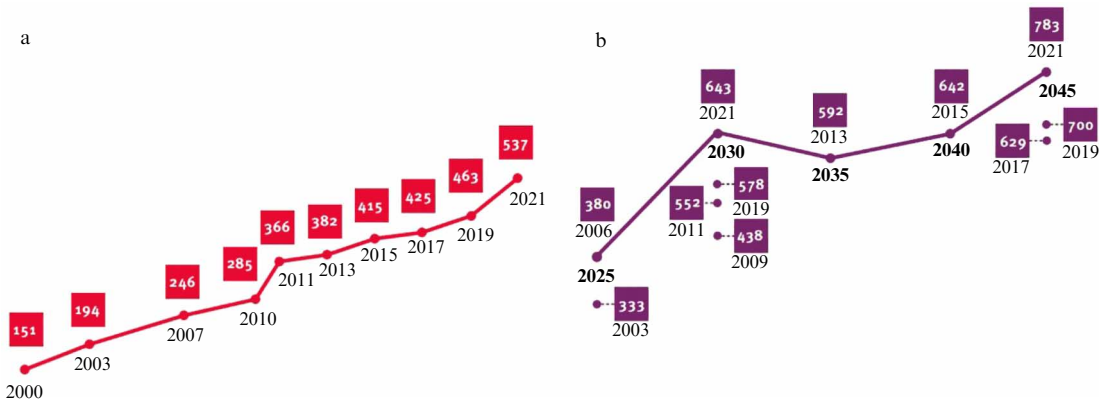

Figure 1. (a) Data on the number of people with diabetes and (b) forecasts for the disease until 2045 according to the 10th edition of the 2021 Diabetes Atlas of the International Diabetes Federation. The year when the forecast was made is shown under the corresponding square.

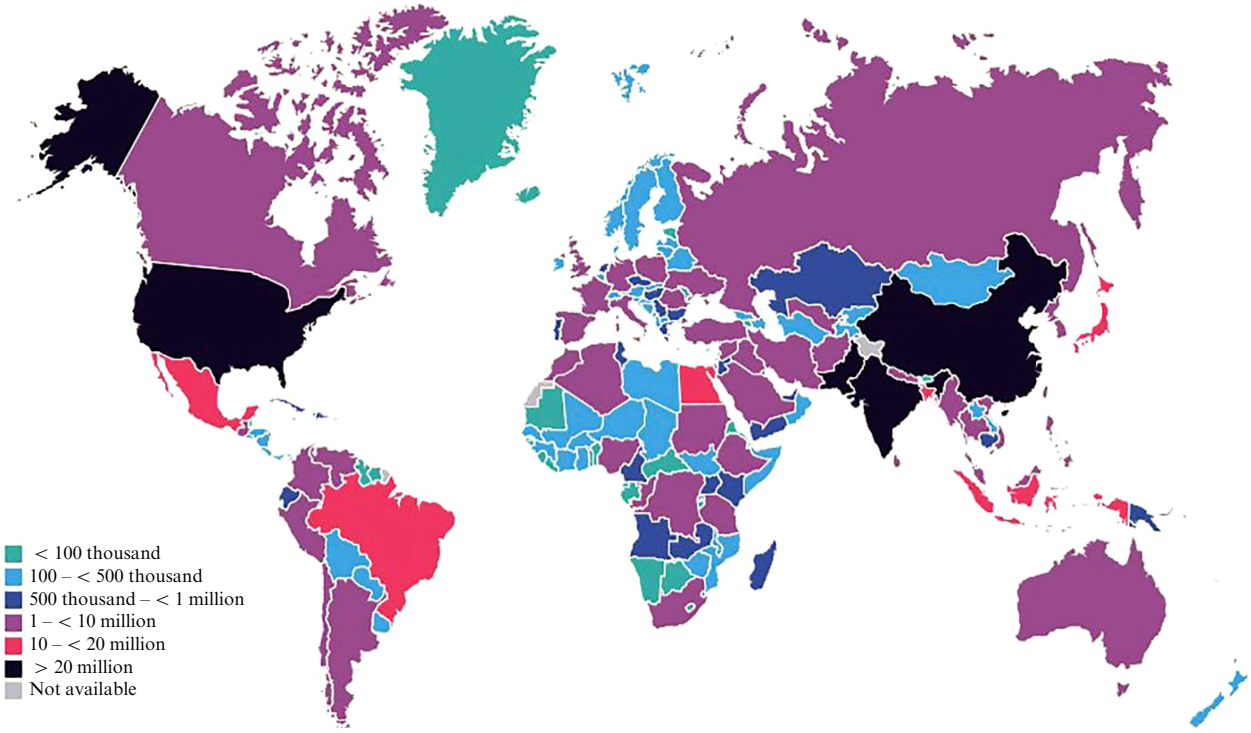

Figure 2. Data on the number of people with diabetes in different countries according to the 10th edition of the 2021 Diabetes Atlas of the International Diabetes Federation.

First-generation blood glucose monitoring systems used oxygen as an electron acceptor, sensing glucose concentrations by either oxygen consumption or hydrogen peroxide production [2]. In 1967, Updike and Hicks [7] proposed an electrochemical biosensor based on enzymes immobilized on the electrode surface. In 1973, Guilbault and Lubrano [8] constructed an enzyme electrode for the determination of glucose by amperometric measurement of the hydrogen peroxide produced. It was not until 1975 that the first sensor for direct glucose measurement was proposed. In fact, Clark and Lyons's technology was transferred to the Yellow Spring Instrument Company, which launched the first glucose analyzer based on a platinum electrode for clinical use.

Figure 3 shows that, starting in the 1960s, the development and application of glucose sensors in the medical field has attracted significant interest in both science and industry. The above-mentioned glucose sensors were the 'first-generation' devices that relied on an oxygen electrode and the production and detection of hydrogen peroxide. The Clark oxygen electrode is a platinum cathode and concentric silver anode that allows oxygen concentration to be measured in a liquid using a catalytic reaction on the platinum surface. In addition, temperature, pH, humidity, and pesticides apparently influence enzyme activity [10]. Disadvantages of using an enzymatic assay for glucose determination are the relatively high cost, time-consuming fabrication of structures, instability, and denaturation of glucose oxidase. To address these issues, a variety of enzyme-free sensors have been explored to improve electrocatalytic activity and selectivity for glucose oxidation, consistent with a move toward 'second generation' glucose sensors.

Intense efforts over the past decades have focused on the development of so-called 'second generation' mediator-based glucose sensors [11, 12], the introduction of commercial glucose meter strips, and the use of further modified electrodes to improve sensor performance [13]. Advances

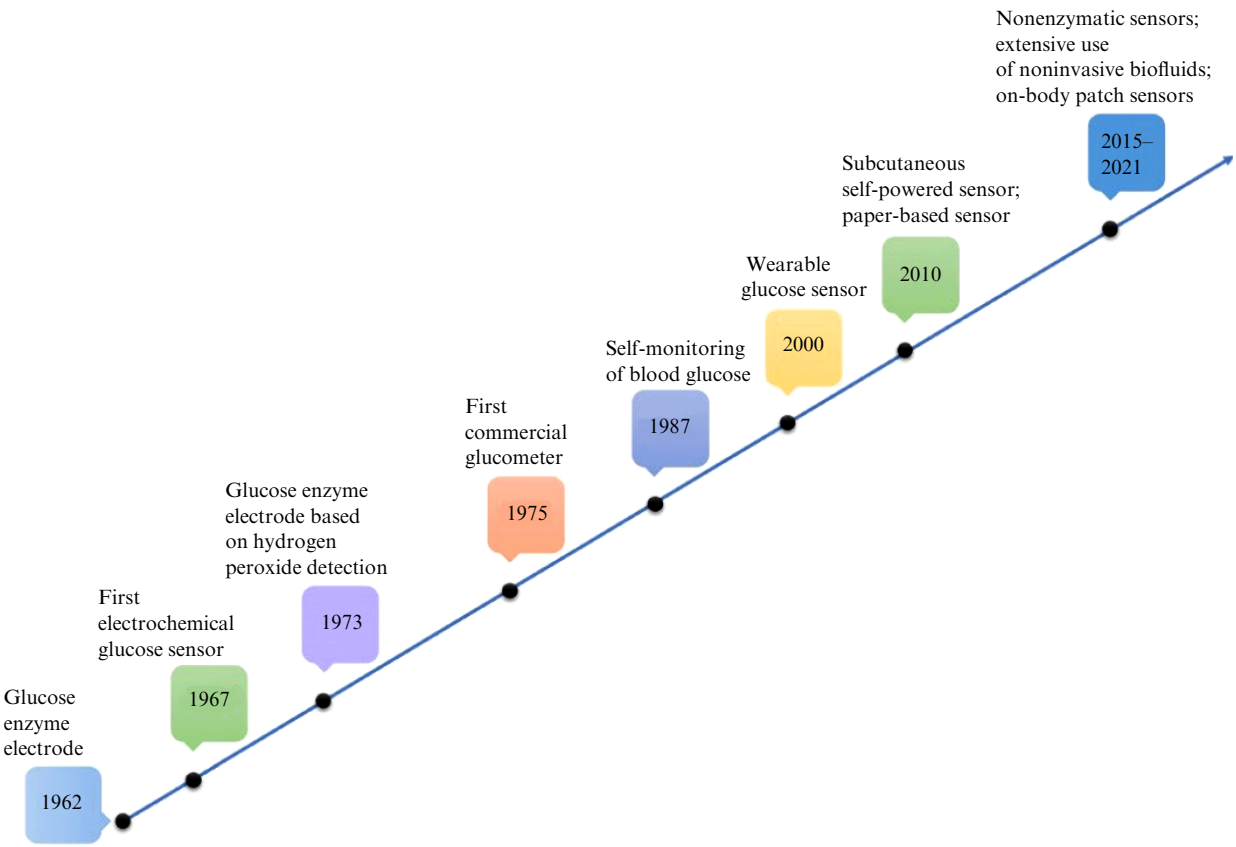

Figure 3. Milestones in the development of glucose sensor systems [4].

have been achieved by replacing oxygen with a synthetic electron acceptor (mediator) capable of transporting electrons from the enzyme center to the electrode surface. A mediator is a low molecular weight analogue of an enzyme. In second-generation enzymatic sensors, enzymes instead of oxygen transfer electrons to artificial electron acceptors to avoid interference from other redox reactions. The reacted artificial electron acceptors are monitored electrochemically. These mediator–based sensors increase the rate of electron transfer between the electrode and the enzyme. Nanostructured metal oxides and semiconductors have been widely explored at this stage to develop biosensors with high sensitivity, fast response time, and stability for glucose detection through electrochemical oxidation. Thus, ZnO, Cu(I)/(II) oxides, MnO_2, TiO_2, CeO_2, SiO_2, ZrO_2, and other metal-oxides were used for glucose biosensors [14]. A nonenzymatic metal-oxide glucose sensor provides cost-effective and direct glucose detection.

Further research was aimed at developing a technology that does not need a mediator to obtain a reagent-free glucose sensor. The 'third generation' of such sensors is based on the direct electron transfer between the enzyme and the electrode without the use of usually toxic artificial mediators. The main advantage is high selectivity, since the working potential is identical to that of the enzyme and is therefore less prone to any interference [4, 11, 12].

Recently, devices based on the direct electrooxidation of glucose have been proposed as a possible 'fourth generation' of sensors, which mainly use noble metals as a catalyst to overcome the limitations posed by conventional enzymatic glucose sensors [15]. Gold and platinum nanoparticles, graphene, graphene oxide and composites based on them, and other carbon materials are used as catalysts [16–23]. Although the goal is to detect glucose in a complex sample matrix (tears, saliva, sweat, and urine), the calibration curve has in most cases been measured in an electrochemical cell using glucose solutions (i.e., alternative conditions).

Below, we will mainly consider third- and fourth-generation noninvasive sensors and glucose-sensing devices that offer a more or less complete set of measurements, from real-time detection to analysis and data transfer to a portable device (for example, a smartphone). For such devices, sweat is the most attractive liquid for analysis. Sweat, in addition to water, includes many constituents, such as oxygen, glucose, insulin, glucagon, cortisol, lactate, adrenaline and alcohol (ethyl), and metal ions (sodium, potassium) [24, 25]. It is known that the concentration of glucose in sweat is approximately an order of magnitude lower than that of glucose in blood [14, 23]. However, the development of wearable sweat sensors has stalled at the experimental and laboratory stages, mainly due to an incomplete understanding of the dynamics of sweat composition and the physiological information contained in sweat. Taking advantage of flexible and hybrid electronics, wearable sweat sensors address this limitation by enabling on-site sweat analysis with real-time feedback, creating opportunities for prevention, timely diagnosis, and treatment.

Figure 4 presents a chart showing the division of glucose measurement methods into two groups: methods that require the use of special equipment (left half of the chart) and cannot be done at home, and personalized medicine methods. For the methods of the first group, it is necessary to note a higher reliability of measurements and a wide range of optical techniques [26–31]. But even if simplified specialized equip-

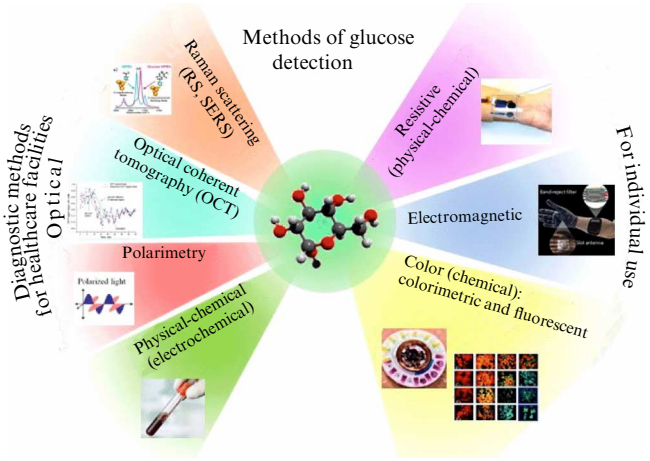

Figure 4. Diagram showing the division of methods for measuring glucose into two groups: on the left, those that require the use of special equipment and are suitable for use in healthcare facilities; on the right, methods for individual use.

ment is developed, these techniques can only be used in health facilities. This review is devoted to the second group of sensors and at-home techniques.

Wearable glucose sensors for personalized diabetes management are considered to be the ones that lack strict evidence that their signal is proportional specifically and only to glucose content in the blood. Such evidence is most likely impossible to obtain, since we are dealing with a human body which is a very complex and multifactorial system. However, if certain monitoring rules are followed and calibration curves are used, as a rule, an individual can fairly reliably assess their condition using data from wearable sensors. Many studies test the response of sensors to glucose solutions in electrochemical cells, and a calibration curve is subsequently used to estimate the glucose content. Let us consider various approaches currently being developed for analyzing glucose (Fig. 4), primarily in sweat and other fluids, as well as methods for transmitting information from the sensor.

2. Optical methods for glucose monitoring

This section will briefly review some of the methods based on the optical response of the sensor: photoluminescence, fluorescence, and surface enhanced Raman scattering (SERS). Approaches such as SERS are highly sensitive but require special equipment. As a result, they fundamentally cannot be brought to the point of testing blood glucose levels using noninvasive at-home methods.

Recently, glucose detection using sensors based on the boric acid molecule and its derivatives have been developed as an alternative to conventional methods. Thus, Alizadeh et al. [24] have recently proposed an optical sensor using fluorescent boron-doped carbon nanoparticles for glucose detection that can be monitored with a smartphone. Glucose selectively leads to aggregation of carbon nanoparticles based on the covalent binding of glucose and boric acid, resulting in a linear increase in fluorescence with increasing glucose concentration (a quantum yield of 46%). The general operation scheme is illustrated in Fig. 5, which shows the use of a synthesized probe with carbon nanoparticles for detecting glucose by photoluminescence intensity. Its variations are monitored by the smartphone camera, and the green channel intensities of the color images are processed using the RGB option of the smartphone. Thus, the method holds great promise as a convenient practical platform for quantifying glucose levels in a serum sample. Carbon nanoparticles are shown to have a linear photoluminescence intensity response range from 32 μM to 2 mM with a detection limit of 8 μM for measuring glucose in diluted serum [24].

Othman et al. [32] used a similar approach, implementing a single-step synthesis of boronic acid using 3-thiophenylboronic acid as the starting material, which effectively interacts with the π electrons of the carbon dot. The chemical sensor for this study was developed using a single-step procedure for doping carbon dots with boron and sulfur (Fig. 6), which ensures effective interaction with glucose [32, 33]. When glucose is added, dipole interaction causes aggregation of carbon dots and fluorescence quenching. The synthesis procedure used requires fewer details and is more efficient from a production point of view, with a quantum yield of 22.6%. The ability to measure glucose concentrations in the range from 1 to 250 μM with a detection limit of 0.57 μM was demonstrated. Fluorescence nanoparticles with boronic acid had excellent selectivity and strongly resisted interference from several other biomolecules (competing saccharides, etc.) that exhibited high selectivity for glucose. The method was demonstrated *in vivo* using human saliva [34]. This approach does not require expensive enzymes or complex surface modification techniques. The developed sensor is highly sensitive to the level of glucose in saliva.

Surface enhanced Raman scattering is extremely sensitive due to signal amplification and the specific manifestations of the molecules of interest. The main SERS-based achievements are presented in reviews [32–36]. As is known, SERS demonstrates the ability to detect various pathogenic bacteria [37], identify fungal diseases [38], and monitor biomarkers of cancer [39] and COVID-19 viruses [40]. Direct SERS-based detection of glucose has been difficult due to the poor adsorption of glucose on metals and the low cross section of glucose. To date, four main approaches have been developed for SERS-based glucose detection, namely, the SERS active platform (increasing the glucose adsorption cross section through additional surface treatment), a partition layer functionalized surface, boronic acid-based sensors, and enzymatic reaction-based biosensors (see Fig. 7 from review [34] for examples of these four approaches; see also [41–44]).

To date, most analytical methods or SERS sensors have been limited to research laboratories, because there are still a number of problems associated with quantitative analysis, stability, and reproducibility. Note that all of the above problems are inherent to varying degrees in all approaches being developed, whether optical, chemical, or physicochemical. In addition, it is important to eliminate noisy and weak signals through data processing, machine learning, and signal combinations [45, 46]. The SERS intensity depends on structural features and fluctuations. Reliability determined by sensor design, careful sample preparation, control of measurement conditions, and adequate data analysis is another challenge that needs to be addressed, and not just for this method.

In general, optical methods can provide higher reliability and unambiguous interpretation compared to wearable glucose sensors. With further improvements, SERS-based glucose sensors through portable Raman scattering-based sensing platforms may hold promise for future use for

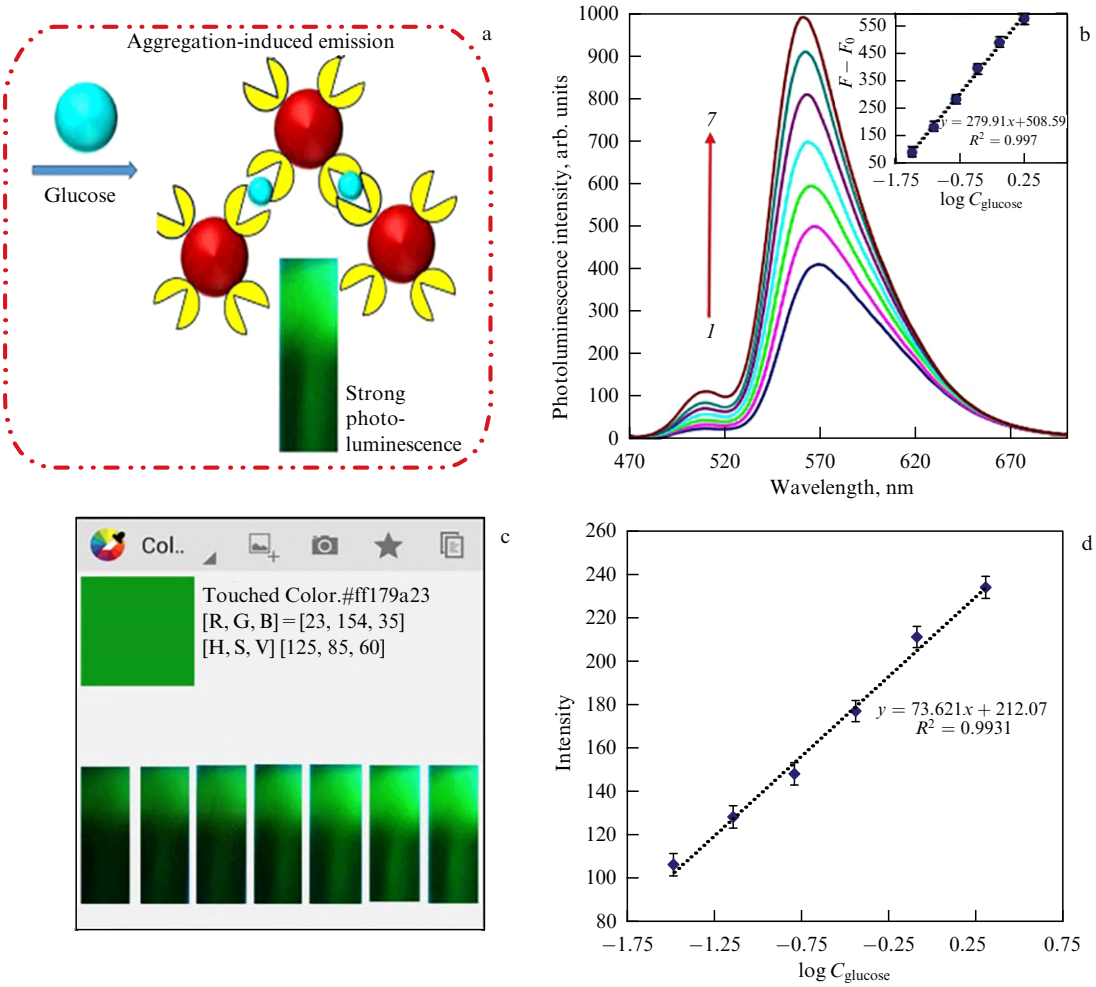

Figure 5. (a) Schematic illustration of fluorometric determination of glucose based on aggregation-induced emission (AIE). (b) Fluorescence responses of the sensor upon addition of various concentrations of glucose: 0.032, 0.05, 0.072, 0.162, 0.364, 0.82, and 2 mM (from *1* to *7*). (c) Fluorescence response of sensor probe to various concentrations of glucose analyzed by a smartphone. (d) Linear calibration plot of green color intensity versus concentration of glucose [24].

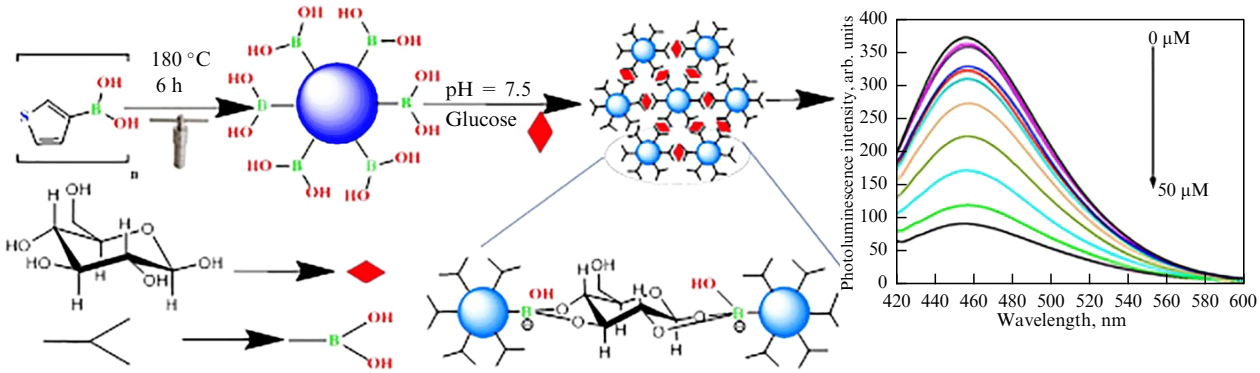

Figure 6. Schematic diagram describing synthesis procedure and application principle of boronic acid functionalized sulfur-doped carbon nanodots for glucose sensing [32].

painless glucose monitoring in diabetic patients in healthcare facilities.

3. Colorimetric, fluorescent, and microfluidic biosensors

Recently, much effort has been invested in the expansion of various approaches to biosensor analysis, including colorimetric and fluorescent visualization of the obtained result.

He et al. [47, 94] demonstrated a set of flexible wearable sensors for measuring pH, sodium chloride, glucose, and calcium, which, in combination with superhydrophobic reservoirs for sweat storage and colorimetric biosensors, enable sweat collection and biodetection using a mobile phone. Figure 8 shows (a) calibration curves with the

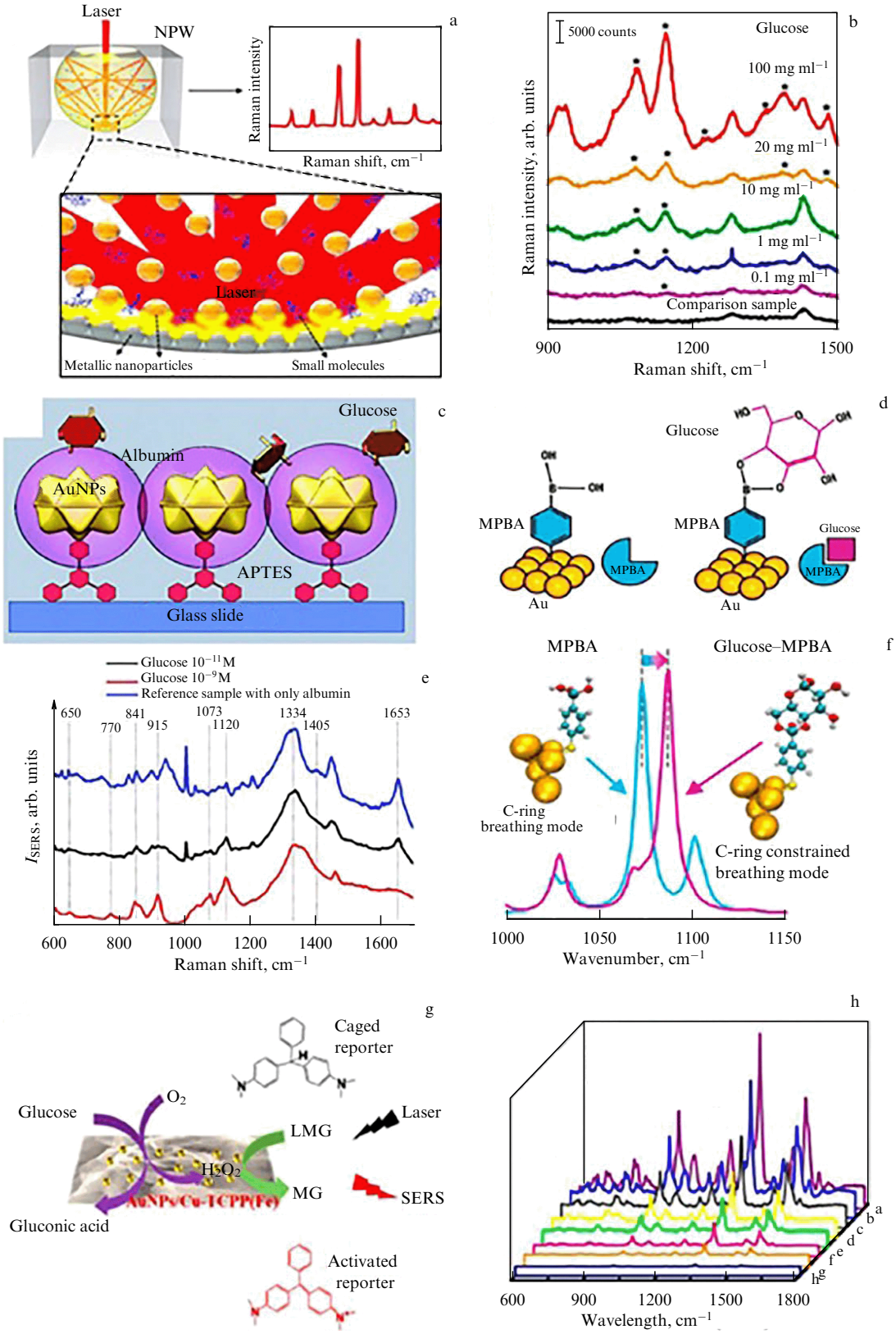

Figure 7. (a) Schematic illustration of solution-state SERS maximized by using a spherical nano-plasmonic well (NPW) with expected enhanced Raman spectrum signals and (b) concentration-dependent intrinsic SERS spectra of glucose from label-free SERS measurement in the NPW [34, 41]. (c, e) Schematic illustration of SERS substrates: (c) functionalization of glass surface with albumin-coated Au nanoparticles and (e) spectra for different glucose concentrations [34, 42], APTES — aminosilane layer. (d, f) Indirect glucose detection using boronic acid-based sensors: (d) schematic illustrations and (f) Raman-peak shifting before and after glucose binding [34, 43], MPBA — $C_6H_7BO_2S$ — mercaptophenylboronic acid. (g) Schematic illustration of enzyme-free tandem reaction strategy for SERS detection of glucose and (h) spectra for glucose concentrations from (a–h): 0.16, 0.32, 0.64, 1.25, 2.5, 5.0, 6.0, and 8.0 mM; inset is the enlarged range from 1300 to 1400 cm^{-1} [34, 44]. LMG and MG are preparations (dyes): leucomalachite green and malachite green.

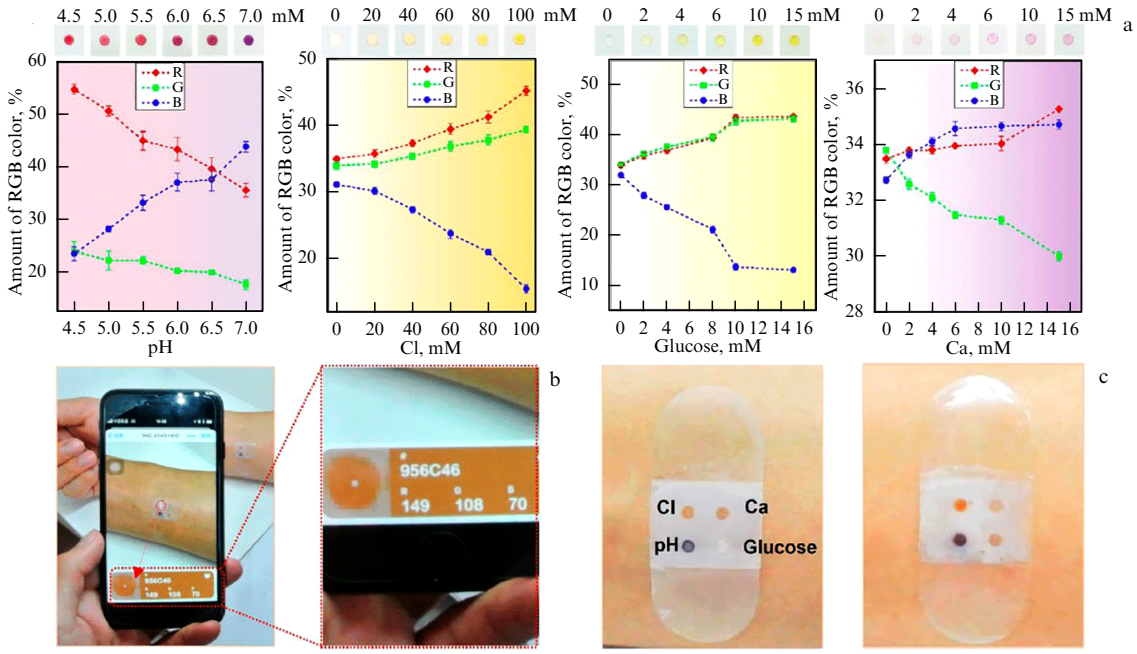

Figure 8. Matrix of four sweat biosensors. (a) Calibration plots of normalized % RGB value *versus* pH, chloride, glucose, and calcium concentrations for quantitative sweat analysis. Each colored dot on the graph vertically matches microdroplets of the gradient concentration above. Colors: R — red, G — green, and B — blue. (b) App-assisted cellphone as screening module capable of adjusting viewing position (white cross) to targeted sites on bands to verify RGB (red, green, and blue) information. (c) Color contrast of superhydrophilic microarray before (left) and after (right) raw sweat excretion [47].

corresponding colored dots above, (b) determination of the colorimetric sensor color change, and (c) images of biosensor matrices. A miniaturized thin plasmonic metasurface with uniformly arranged mushroom-shaped particles was designed and integrated into a microfluidics platform, resulting in SERS. Compared with conventional wearable platforms, the microfluidic SERS system allows sweat to be analyzed with high temporal resolution, providing up-to-date SERS analysis. A portable and customized Raman analyzer with a human-friendly machine interface is suitable for portable recognition of spectroscopic biomarkers in sweat and holds promise for personalized medicine. An advantage of this approach is clear visualization of the signal and, accordingly, the absence of the need for data transmission. Wearable colorimetric sweat sensors offer access to visual perception by observing the color depth/absorbance/fluorescence caused by the chromogenic reaction between the indicator and glucose or other test substances.

Koh et al. [48] reported a type of soft, wearable, microfluidic device that can directly and reliably collect sweat from pores on the skin surface. The device collects sweat into various channels and reservoirs for multi-parametric determination of biomarkers of interest [total water loss (sweat) and concentrations of lactate, glucose, creatinine, chloride ions, and pH], with options for wireless interfaces to external devices for image capture and analysis. The devices can mount at multiple locations on the body without chemical or physical irritation by use of biocompatible adhesives and soft device mechanics, including flexible and stretchable sensors, and watertight interfaces. These devices measure total sweat loss, pH, lactate, sodium chloride, and glucose concentrations by colorimetric detection using near-field communication (NFC) electronics for wireless data transmission. An NFC module ($\sim$ 0.1 g) supports both wireless power delivery and short-range (10 cm) data transfer to any consumer device such as a smartphone, tablet, or smart watch. Tests included two human trials: a controlled, indoor, mild sweat-inducing study, and a 'real-world,' outdoor-use study conducted during a long-distance bicycling race [48]. Polydimethylsiloxane (PDMS), used as the basis of the structure, is attractive for this application, including optical transparency, ease of patterning into microfluidic systems, biocompatibility, flexibility, and high elasticity ($\sim$ 200% strain at break). Glucose concentration is analyzed by an enzymatic reaction of glucose oxidase physically immobilized in a cellulose matrix. During the reaction, glucose oxidase produces hydrogen peroxide, associated with the oxidation of glucose and a reduction in oxygen. After this reaction, iodide oxidizes to iodine by peroxidase, resulting in a change of color from yellow (iodide) to brown (iodine) to an extent defined by the glucose concentration. Note that glucose concentration in sweat is usually an order of magnitude lower than in plasma; the range of sensitivity in the described devices allows hyperglycemia to be diagnosed.

Xiao et al. [49] reported a microfluidic chip-based wearable colorimetric sensor for detecting sweat glucose. The device consists of five microfluidic channels branching out from the center and connected to microdetection chambers (Fig. 9). The microchannels route the sweat excreted from the skin into the microchambers, and each one is integrated with a check valve to avoid the risk of backflow of chemicals from the microchamber. The microchambers contain pre-embedded glucose oxidase (GOx)–peroxidase–o-dianisidine reagents for sensing glucose in sweat. It was found that the color change caused by the enzymatic oxidation of o-dianisidine may exhibit a more sensitive response to glucose than the conventional GOx–peroxidase system. These sensors can perform five parallel detections at a time (humidity, pH, potassium, sodium, and glucose). The resulting linear range for sweat glucose was 0.1–0.5 mM with a detection limit of 0.03 mM. The sensor was used to determine the glucose content in sweat samples for a

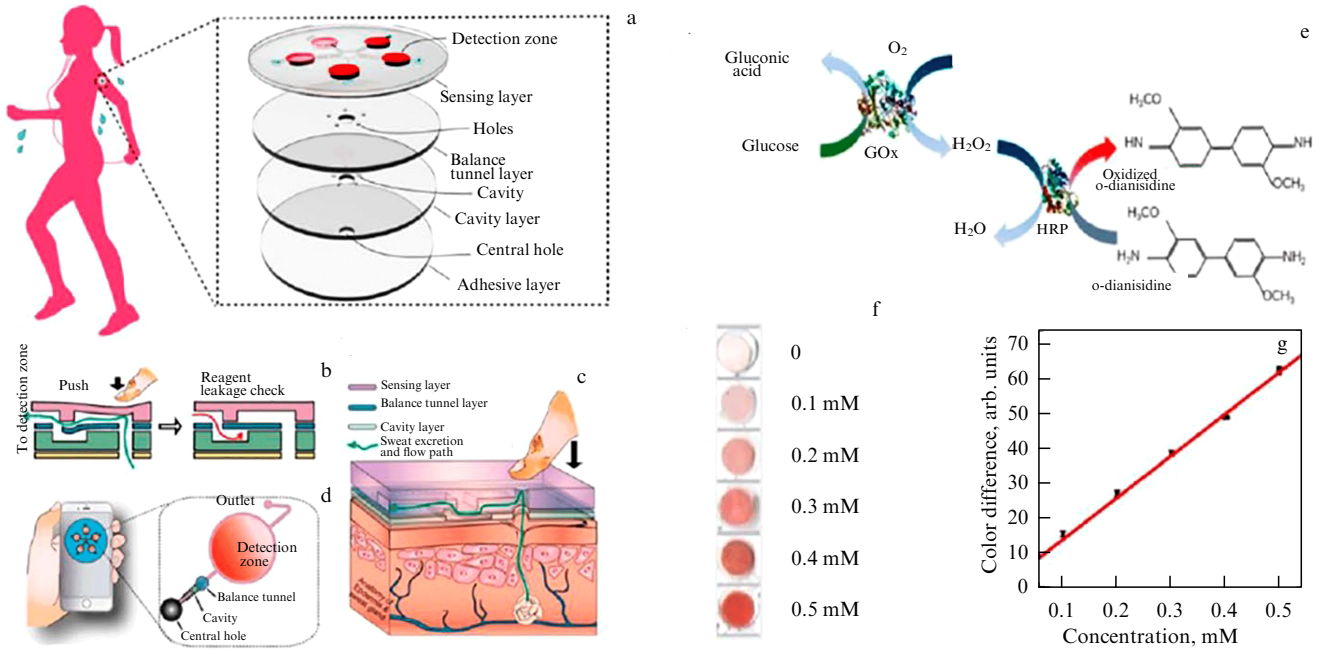

Figure 9. Wearable colorimetric microfluidic chip-based sensor for glucose detection. (a) Schematic of a sensor composed of four layers that facilitate sweat to flow from skin's surface to five detection chambers containing pre-embedded colorimetric reagents in the top layer. (b) Schematic drawing of structure and function of integrated microfluidic check valve. (c) Illustration of sweat secretion from human eccrine gland and sweat collection by the sensor. (d) Illustration of smart phone-based data visualization and acquisition of sweat glucose detection. (e) Schematic illustration of chromogenic reaction of the GOD–peroxidase–o-dianisidine system. HRP — peroxidase. (f) Colorimetric responses of the GOD–peroxidase–o-dianisidine system toward glucose with various concentrations from 0.10 to 0.50 mM. (g) Linear relationship between color difference and glucose concentration [49].

group of subjects. The results showed that this wearable colorimetric sensor could detect subtle differences existing in the sweat glucose concentration [49].

A solution containing glucose can cause a color change in the microchamber through the catalytic reaction shown in Fig. 9e. Glucose oxidizes by GOx in combination with oxygen reduction and the formation of H_2O_2. Then, the resulting H_2O_2 oxidizes colorless o-dianisidine to form red oxidized o-dianisidine. Figure 9f shows the color change of the microchamber in response to glucose. The presence of glucose was found to impart a red color to the GOx–peroxidase–o-dianisidine system, in which the color increased in proportion to increasing glucose concentration. The color change is visible to the naked eye even at a glucose concentration of only 0.1 mM. In comparison with the GOx–peroxidase–KI system, the color change (from I^- to I_2) upon glucose administration was difficult to detect at glucose concentrations less than 0.3 mM. This is consistent with previous reports that the GOx–peroxidase–KI system could detect glucose concentrations higher than 0.2 mM [50, 51]. The low sensitivity of the KI system may be due to the reducing property of iodine, which easily oxidizes when exposed to oxygen. Thus, compared with the GOx–peroxidase–KI system, the GOx–peroxidase–dianisidine system is more suitable for the detection of glucose in low concentrations, such as sweat glucose.

Bandodkar et al. [52] reported a hybrid, two-component, battery-free, skin-interfaced system for detecting sweat parameters. The system includes a disposable, soft, microfluidic network and a thin reusable NFC electronic module. A component view of the overall construction of each of these subsystems is shown in Fig. 10a. A flexible silicone elastomer was used to pattern a set of chambers, channels, and valves for colorimetric sweat sensing. The adhesive layer ensures not only robust attachment to the skin but also a sweat route in the bottom side of the microfluidic structure. The soft flexible construction as shown in Fig. 10b allows comfortable watertight mounting on curved regions of the body.

Figure 10c shows an electronic module that exploits a detachable, bilayer, flexible, printed circuit board (diameter, 18 mm, thickness, ~ 0.5 mm) with a minimum number of components for real-time data acquisition from biofuel cell-based lactate and glucose sensors (diameter, 32 mm; thickness, ~ 1 mm). Estimates show that this platform (~ 1 g) is almost 20 times lighter in weight and four times smaller in size of sensor systems based on battery-powered Bluetooth radios [53, 54].

Electrochemical biofuel cell-based glucose sensors have the following design. The anode consists of a circularly cut carbon nanotube (CNT) or graphene paper that provides a conductive large-surface area substrate to immobilize the GOx enzyme and to shuttle electrons between the enzyme's active sites and the conductive electrode. Often, to prevent sensor saturation and expand the detection limit into the physiological range, a diffusion barrier (a film of porous material, such as Nafion) is used. Side effects of such a barrier include reduced sensor sensitivity and increased response time. A chitosan and polyvinyl chloride (PVC) membrane covers the anode to minimize leaching of the mediator and enzyme and to extend the linear detection range of the sensor. The cathode consists of a functionalized platinum-coated gold current collector and a Nafion protective membrane. The platinum black acts as a catalyst for oxygen reduction and the Nafion membrane prevents leaching of the platinum black. The fluoride backbone of the Nafion polymer facilitates adsorption of dissolved oxygen on the cathode surface, thereby improving the kinetic rate of oxygen reduction. A resistor connected across the sensor transforms the current

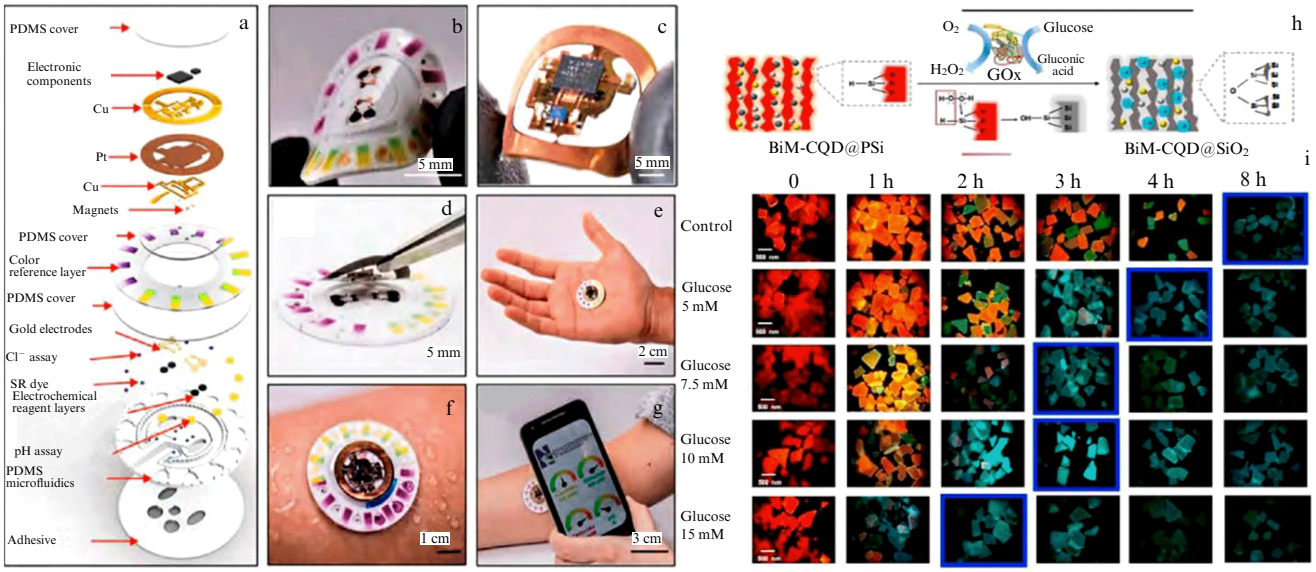

Figure 10. Schematics of sensing devices from Refs [52] and [55]. (a) Schematic illustrating exploded view of the complete hybrid battery-free system. PDMS — polydimethylsiloxane. Close-up images of (b) a microfluidic patch with embedded sensors and (c) battery-free NFC electronics. (d) Image illustrating reversible magnetic attachment of NFC electronics to the microfluidic patch. (e) Image of complete system. (f) Image illustrating the device when sweating. (g) Phone interface illustrating wireless communication and image acquisition [52]. (h) Diagram of glucose monitoring using BiM-CQDs@PSi fluorescence stimulated by H_2O_2 generated by glucose oxidation with GOx catalyst. (i) Fluorescence images of BiM-CQDs@PSi particles in simulated sweat aqueous with different concentration of GOx. Images with first appearance of complete blue fluorescence are marked by blue borders [55].

into a voltage-based signal for detection and wireless transmission *via* NFC electronics. The output voltage of biofuel cell-based sensors increases linearly with increasing load. However, at higher loads, the response time also increases. Therefore, the selection of external load resistance for glucose sensors is based on the need to generate a voltage signal in the range of 0 to 1 V (measuring range for the NFC chip).

The advantage of the presented system is the ease with which it can be worn. In addition, the developed microfluidic structure allows working with sweat samples without cross-talk between different sensors. The design of a biofuel cell includes a voltage amplifier with a certain load on the sensing element, implemented using a small operational amplifier and miniature passive components. The circuit processes the signal for digitization in the built-in NFC chip. Analog electronics are reliable, with minimal susceptibility to external interference associated with NFC electronics and supply voltage fluctuations [52].

Cui et al. [55] reported noninvasive and visual monitoring of sweat glucose using a wearable skin pad based on a fluorescent active layer (CQDs@PSi). A CQDs@PSi layer includes carbon quantum dots (CQDs) and luminescent porous silicon (PSi) particles. To improve glucose detection sensitivity, the PSi surface is modified using bimetallic nanoparticles (BiM) of gold and silver nanoparticles, thereby enhancing the fluorescence intensity triggered by hydrogen peroxide (H_2O_2). The wearable skin pad can be fabricated by combined immobilization of newly prepared BiM-CQDs@PSi and glucose oxidase (GOx) in a transparent and biocompatible chitosan film supported by an adhesive polyurethane membrane. Due to the interaction of the components, the blue fluorescence of the CQD is quenched, and the red fluorescence from the PSi first appears on the sensor. When the skin pad is attached to the body, the amount of H_2O_2 increases due to the GOx-catalyzed oxidation of glucose, which promotes the oxidation of PSi. This leads to the decay of PSi fluorescence and the recovery of CQD fluorescence, making the color change from red to blue. The process is shown schematically in Fig. 10a. In addition, the kinetics of changes in the fluorescence (red-blue) is proportional to the concentration of sweat glucose (Fig. 10b). Using photos taken with a smartphone, a simple data processing algorithm was developed and clinical tests with regard to diabetics and healthy volunteers were implemented. The described noninvasive visual system for monitoring sweat glucose clearly indicates hyperglycemia [55].

Recent technological advances in wearable sensors have made it easier to detect sweat components. A critical bottleneck for sweat analysis is achieving uniform high-throughput fabrication of sweat sensor components, including the microfluidic chip and sensing electrodes. Nyein et al. [56] presented microfluidic sensors mass-produced via roll-to-roll printing processes. Figure 11 shows printed structures that can be attached to different parts of human skin using a patch. The patch allows sweat to be captured within a spiral microfluidic system for real-time measurement of sweat parameters, including Na^+, K^+, and glucose, and identification of relationships between sweat parameters and blood glucose dynamics in healthy people and people with diabetes. By providing a comprehensive analysis of sweat, the presented device is an important tool in progressing towards personalized point-of-care health and fitness monitoring.

The patch shown in Fig. 11c measures total admittance between parallel spiral silver electrodes contained in a microfluidic channel. As the fluid flows along the channel, admittance between the two electrodes increases due to increasing conductivity, creating a relationship between admittance and the encapsulated fluid volume. The sweat sensing patch presented here allows for immediate and

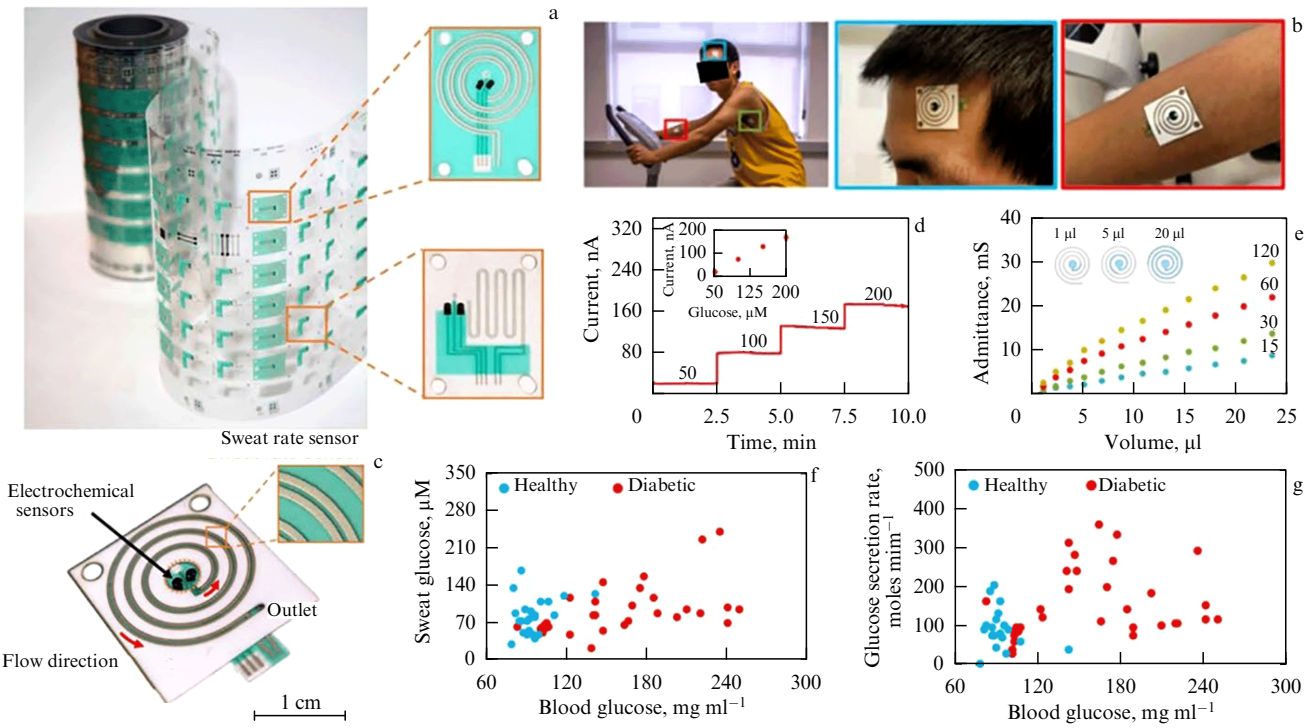

Figure 11. Schematics of fabricated sweat sensing patches for sweat analysis. (a) Roll-to-roll rotary screen printing of a wearable biosensing patch and (b) optical image of sensing electrode patterns attached to human body. (c) Assembled biosensing patch with electrochemical sensors contained within the collection reservoir, and with an electrical sweat rate sensor embedded in the microfluidic channel. Biosensor patch is assembled by combining a sensing layer, a microfluidic adhesive spacer, and a PET cover sheet. (d, e) Characteristics of glucose sensors and relationship between fluid volume contained in the microfluidic channel and admittance measured across Ag sweat rate electrodes in 15 to 120 mM NaCl solutions. (f, g) Average levels of sweat glucose and average sweat glucose secretion rate versus blood glucose of 20 healthy and 28 diabetic subjects [56].

accurate glucose measurements from sweat analysis, making it possible to investigate precise basal sweat-to-blood glucose correlations. For each subject, studies were conducted on the rate of sweat response to blood glucose changes. The glucose sensor response time was about a minute after the sensor surface was covered with sweat, which occurs within a few minutes after the onset of sweating. Figure 11g shows the result of comparing the mean sweat glucose concentration with the blood glucose level in all subjects. Overall, there is significant variability in the data, indicating that sweat glucose concentrations obtained using sweat storage (sweat is first accumulated in a ~ 2.5 μL reservoir and then travels within a spiral microfluidic channel) do not reliably predict blood glucose levels.

4. Using antennas for glucose detection

The authors of Refs [57–62] proposed a new and highly sensitive noninvasive wearable multisensing system for continuous glycemic monitoring using electromagnetic sensors. Electromagnetic sensors are typically metallic or graphene devices [50] designed for radiating or receiving electromagnetic waves. The glucose level can be determined using the S parameters of electromagnetic waves transmitted by sensors (S_{11} is the wave reflection coefficient, and S_{21} is the input–output wave transmission coefficient) [57–59]. The sensing system measures variations in glucose levels based on complex changes in the permittivity along the signal path. Thus, the permittivity of blood can change significantly with changes in blood glucose. The sensing system proposed, for example, by Saha et al. [57] uses two mutually directed microstrip patch antennas operating at 60 GHz, which are placed across interrogated samples. The measured transmission coefficient depends on the change in permittivity along the signal path, which includes blood vessels. In test solutions, the system demonstrated a good correlation between the change in reflection coefficient of the S_{21} wave and the glucose level (a S_{21} shift of 0.25 dB corresponded to a glucose level of 5.5 mM). In human experiments, the authors reported a good correlation between changes in the S_{21} parameter and glucose levels in only 20% of participants, which was explained by the high sensitivity of the system to slight hand movements during measurements.

Figure 12 shows the results of testing the reflection coefficient of the S_{11} wave of flexible electromagnetic sensors from [58]. The system is composed of two sensors: a multiband slot antenna and a multiband rejection filter (Figs 12a and 12b). The proposed sensors operate in the UHF and microwave ranges from 500 MHz to 3 GHz. This frequency range allows veins and arteries to be reached through layers of skin, muscle, and fat tissue, while maintaining good sensitivity.

The antennas proposed by the authors mimic the vasculature anatomy. It was shown that, by concentrating electromagnetic waves directly on the blood network, it was possible to attain a higher sensitivity of the sensors. In addition, the proposed antennas were designed for a load corresponding to a human hand. This approach is superior to traditional antenna designs, which suffer from strong reflection of incident waves when placed in contact with the human body at the air–skin interface. Matching the antenna to the human body is of utmost importance. The ability to customize the filter is an important aspect, adding another degree of freedom to the design and allowing the sensor

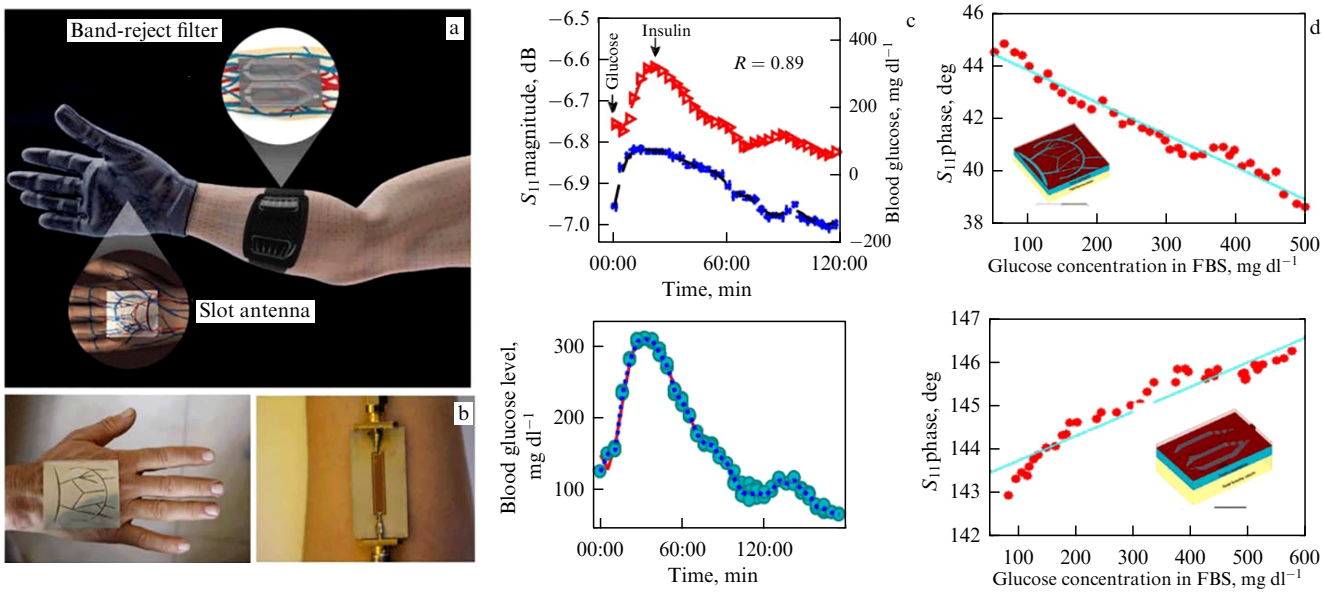

Figure 12. (a) Electromagnetic sensor mimicking vasculature anatomy. (b) Prototype of antenna slots and filter for transmitting data. Proposed sensors operate at UHF and microwave bands, ensuring sufficient electromagnetic wave penetration depth to reach targeted veins and arteries. (c) Top: Rigid filter's S_{11} parameter magnitude response versus actual blood glucose level at 1.57 GHz. Bottom: Estimated glucose level versus time. Rats were used in the experiments; to convert glucose level to mM, values on the axis must be divided by 18. (d) Antenna's response S_{11} phase versus the reference glucose level for a slot antenna and a filter [58]. FBS — fetal bovine serum.

system to be further tailored to better accommodate specific individual characteristics. As a proof of concept, the prototype is designed to mimic the blood network in two different locations: the hand and the arm (Fig. 12b). The designed antenna is integrated as part of a wearable glove which senses the vasculature of the hand, and the filter is integrated into the arm band. This incorporation of sensing components in multiple locations enables higher accuracy and faster responsiveness in monitoring blood sugar levels. As a result, this work shows a good correlation between changes in reflection coefficient S_{11} and sugar levels for all subjects.

Omer et al. [63] presented a new design of a portable planar microwave sensor for fast, accurate, and noninvasive monitoring of blood glucose levels. The sensor design includes four hexagonal-shaped complementary slit ring resonators (CSRRs) etched to a depth of 35 μm in a honeycomb-like copper dielectric substrate (Fig. 13). The CSRR sensing elements are coupled *via* a planar microstripline to a radar board operating in the 2.4–2.5 GHz frequency range. The sensor's high sensitivity is attributed to the advanced design of the CSRR sensing elements, which expose glucose samples to intense interaction with electromagnetic fields concentrated around the sensing region at induced resonances. This feature allows the developed sensor to detect extremely subtle variations in the electromagnetic properties that characterize varying-level glucose samples. The desired performance of the fabricated sensor is practically validated through *in vitro* measurements using a convenient setup of a vector network analyzer (VNA) that records a noticeable frequency shift when the sensor is loaded with samples with 70–120 mg dl^{-1} (3.9–6.7 mM) glucose concentrations. The use of the radar demonstrates the dependence of the signal on glucose levels. Additionally, differences in sensor responses for the tested glucose samples are quantified by applying the principal component analysis machine learning algorithm. The proposed sensor has other attractive characteristics, including compact size, ease of manufacture, affordable cost, nonionizing nature of exposure, and minimal health risk, making the proposed sensor a possible candidate for noninvasive glucose monitoring in diabetes, as evidenced by preliminary results from an *in vivo* experiment of monitoring human blood sugar levels by placing a fingertip on the sensor. The presented system is a developmental platform toward radar-driven wearable sensors.

5. Sweat-based glucose sensors

Wearable glucose sensors enable the monitoring of various body fluids, such as sweat [64], saliva [65], and tears [66]. However, more and more researchers are inclined to rely on sweat analysis. Sweat consists of 98% water, and the remaining 2% contains about 250 chemical compounds. They are organic components (glucose, lactate, cholesterol, amino acids, etc.) and substances that are formed during the breakdown of proteins, such as lactic acid, urea, ammonia, creatinine, and products of mineral metabolism (phosphates, potassium chloride, calcium salts, and Na^+ and K^+ ions). Since the skin is negatively charged, it has selective permeability to positive ions, neutral molecules, and especially polar molecules [67, 68]. Continued innovation to develop new signal readout techniques is necessary to enable selective component testing and the development of reliable wearable sweat sensors [69].

Research papers examining wearable sweat glucose sensors are more common than those devoted to detection of other body fluids [70–74], because sweat is more accessible and less painful to use. Despite all these advantages, there are some disadvantages/challenges in using wearable sweat glucose sensors. Without sweat stimulation, sampling throughout the day will be irregular [75] and sample production rates will be extremely low [76]. A method to overcome these problems is to increase the sensitivity of the sweat glucose sensor so that the volume of fluid samples

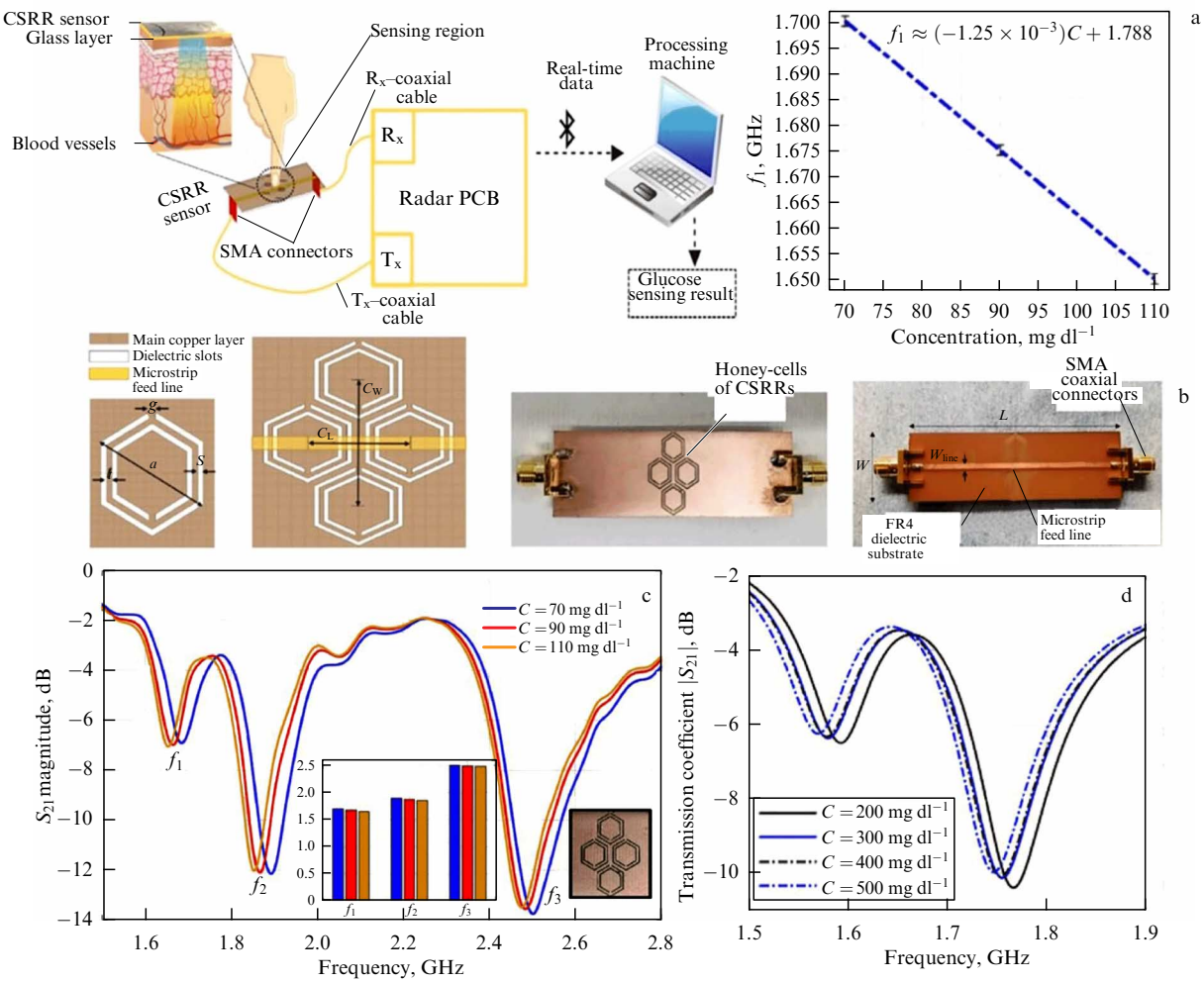

Figure 13. (a) General conceptual illustration of a portable radar-driven sensor for measuring the glucose level noninvasively from the fingertip by sending electromagnetic waves of small wavelength into blood vessels. (b) Configuration of CSRR sensing elements etched at a depth of 35 μm in a copper plate of a dielectric printed circuit board (PCB) (top view). Also shown are topology of hexagonal unit-cell with geometrical parameters, sensor prototype, and microstrip-line used to excite CSRRs. (c) Resonance frequency as a function of blood glucose level. (d) Measured transmission response S_{21} as function of frequency for tested glucose samples of various concentrations [63].

required for glucose detection can be reduced. To increase sensitivity, researchers try to use thinner, more sensitive layers of 2D materials so that the size of the sweat glucose sensors is reduced.

Karpova et al. [77] proposed diabetes monitoring through continuous analysis of undiluted sweat immediately after its excretion using a flow-through glucose biosensor. The biosensors in question are based on Prussian blue and glucose oxidase immobilized in siloxane gel. A peculiarity of Prussian blue is that it is sensitive to hydrogen peroxide and can be used to effectively convert a chemical signal proportional to the amount of hydrogen peroxide into an electrical signal. The composite in use makes it possible to effectively replace a less stable substance in the sensor structure — enzyme pyroxidase. Thus, the combination of Prussian blue and glucose oxidase leads to an enhanced response of the sensor to glucose due to the higher biocatalytic activity of the composite. The calibration range is from 1 μM to 1 mM (flow regime). A correlation is shown between the rates of glucose concentration increase in blood and in noninvasively collected sweat. The dynamics of glucose concentration in sweat, recorded using the proposed biosensor, is in good agreement with the dynamics of blood glucose without a time delay, which opens up prospects for noninvasive monitoring of diabetes. However, this sensor requires sweat stimulation, which significantly limits its application.

The main trend in the development of wearable glucose sensors is the increasing use of inorganic materials such as graphene and metallic nanoparticles [78–85]. In this case, sensing layers, as a rule, have a much smaller thickness and greater sensitivity, which makes them promising for the development of wearable glucose sensors. As a result, so-called resistive or electrochemical sensors have recently been actively developed. Electrochemical sensors are widely used to analyze sweat by converting target contents into currents or potential signals on the miniature and activated electrode surfaces. Such sensors are characterized by high sensitivity and selectivity, while the electrodes can also have a flexible design of various shapes and sizes. Each glucose detection method has its own advantages and disadvantages.

Paper-based substrates are one of the optimal base materials for wearable glucose sensors, and there are many developments on wearable filter paper-based glucose sensors (e.g., [69, 70, 86, 87]). Zhang et al. [87] developed an inexpensive and convenient wearable filter sensor for determining sweat glucose levels. A gold/multiwalled carbon

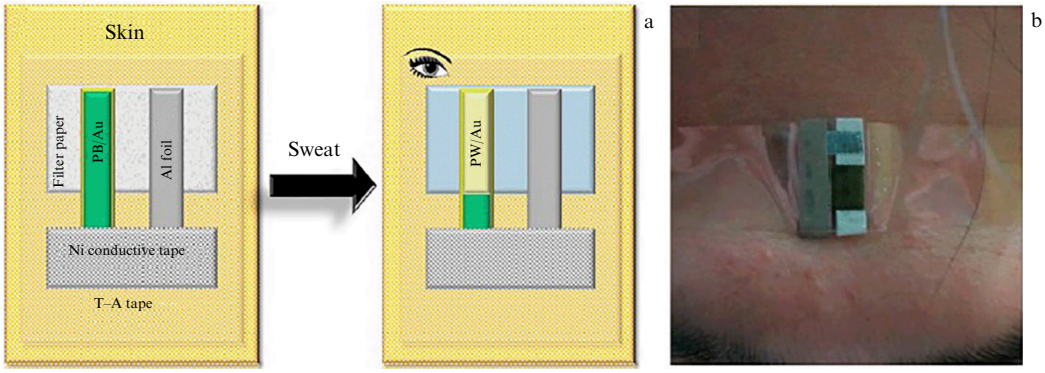

Figure 14. (a) Typical construction of wearable sweat glucose sensor and (b) photo of the constructed sensor on volunteer's hand (borrowed from paper [87]).

nanotube (MWCNT) and glucose dehydrogenase electrode was used to monitor sweat glucose levels. The use of gold and Prussian blue indicating electrodes allowed users to monitor color changes (visualization of the interaction of Prussian blue with glucose) as an indication of glucose levels. As a result, there was no need for other tools, reducing the weight and cost of the sensor. Sempionatto et al. [88] demonstrated a fast and reliable approach that combines a touch-based fingertip sweat electrochemical sensor (PVA gel with GOx on a filter) and a simple testing protocol that leverages the fast sweat rate on the fingertip for rapid assays of natural perspiration, without any sweat stimulation, along with personalized sweat response-to-blood glucose concentration translation.

Wearable sensors are often made in the form of an electrochemical sensor with modified electrodes on a porous base impregnated with various gels (Fig. 14) or organic material, usually including glucose oxidase. The sweat collected by such a substance changes that substance's conductivity due to chemical reactions. The resulting amperometric characteristic is used to analyze the composition of the sweat and, in particular, to determine the glucose concentration.

Skin activity and the ability to control perspiration create important conditions for the operation of wearable sensors. Graphene electronic tattoos or sensing structures applied to the surface of a flexible substrate and glued to the skin are ideal for the implementation of wearable sensors [88]. It should be noted that flexible sensors designed as filamentary serpentines are known to demonstrate significantly greater stability without fracture or delamination [89, 90].

Wearable sensor technologies are of great importance for the implementation of personalized healthcare through continuous monitoring of human health. Human sweat is rich in physiological information and enables noninvasive monitoring. Previously, noninvasive biosensors were described that can only monitor one substance during measurements or that lack *in-situ* signal processing circuitry and sensor calibration mechanisms for accurate analysis of physiological states [47, 91–94]. Given the complexity of sweat secretion, simultaneous and comprehensive screening of a series of biomarkers is critical and requires full system integration to ensure accurate measurements. Bandodkar et al. [91] reported a mechanically flexible and fully integrated sensor array for comprehensive *in situ* sweat analysis, simultaneously detecting sweat constituents such as glucose and lactate, sodium and potassium ions, and skin temperature to calibrate the sensor response. Figure 15 shows a general view of a set of sensors for monitoring glucose, lactose, K^+ and Na^+ ions. The glucose sensor was made by applying a drop of a glucose solution of oxidase/chitosan/carbon nanotubes to a Prussian blue/Au electrode. The transceiver provides wireless data transmission to a Bluetooth-enabled mobile phone using a specially designed application containing a convenient interface for sharing data via email, SMS, etc. or uploading data to cloud servers.

Thus, Gao et al. [93] merged five different plastic-based sensors with conventional commercially available integrated circuit components (more than ten chips) not only to measure the output signal of the sensor array but also to obtain an accurate estimate by processing and transmitting signals about the physiological state of the subjects. The developed sensor bridges the technological gaps among signal conversion, amplification, and filtering, as well as processing and wireless transmission in wearable biosensors. Merging plastic-based sensors that interface with the skin with silicon integrated circuits on a flexible printed circuit board allows complex signal processing. Overall, this platform enables a wide range of personalized diagnostic and physiological monitoring applications.

Lee et al. [95] presented a wearable/disposable sweat-based glucose monitoring device with a feedback multistage transdermal drug delivery module. Careful multilayer patch design and miniaturization of sensors improve the efficiency of sweat collection and the sensing process. Multimodal glucose sensing using glucose oxidase, as well as its real-time correction based on pH, temperature, and humidity measurements, maximizes the accuracy of the sensing. A porous sweat-uptake layer is placed on Nafion and sensors. Figure 16 shows images of two variants of disposable wearable devices on different substrates for monitoring sweat and detecting glucose concentration. Reducing the size of the sensors leads to a decrease in the required amount of sweat. The sensors are calibrated using an electrochemical cell. When analyzing the measurement results, the concentration of glucose in the blood is assumed to be an order of magnitude higher than in sweat (see, for example, Refs [14, 23]).

Pu et al. [96] reported a thermal activated and differential self-calibrated flexible epidermal biomicrofluidic (extraction of intercellular fluid) device for wearable accurate blood glucose monitoring. They proposed an Na^+ sensor and a correction model to eliminate the effect of individual differences that lead to fluctuations in the amount of interstitial fluid extraction. An electrochemical sensor (Fig. 17) with a three-dimensional nanostructured working

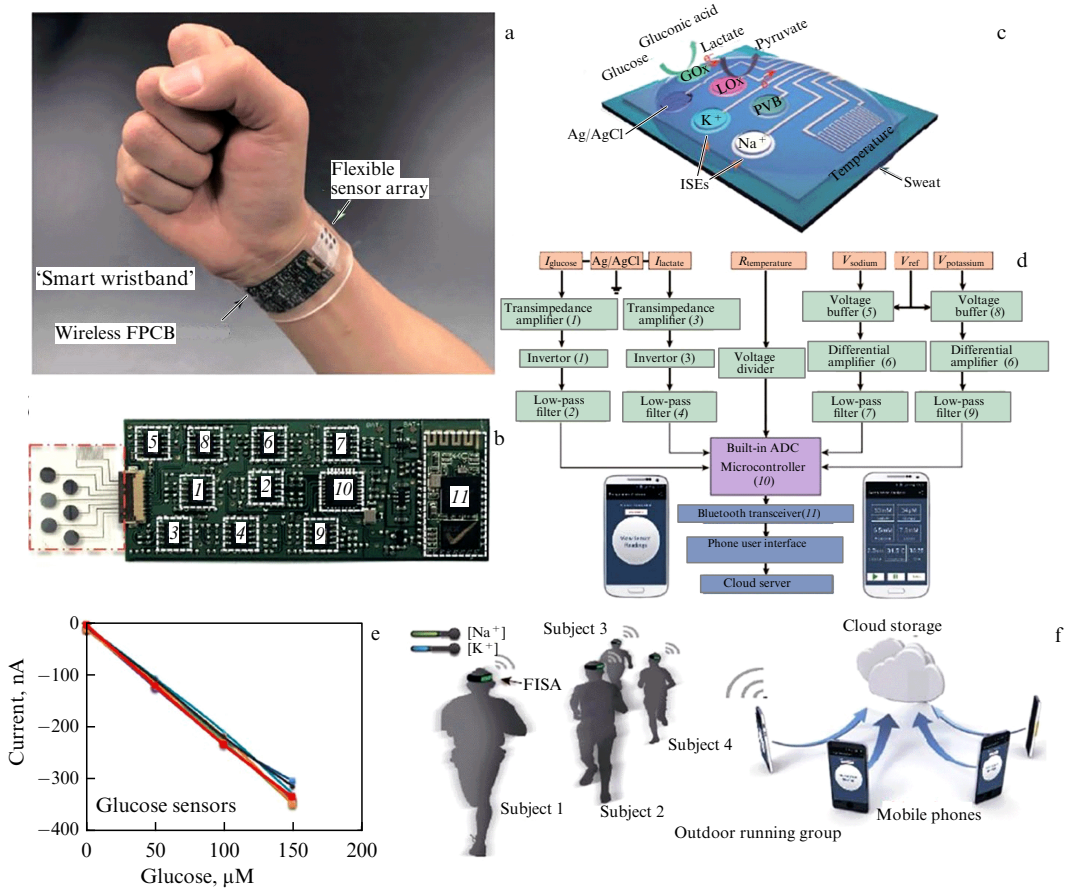

Figure 15. Images and schematic illustrations of a flexible integrated sensing array (FISA) for multiplexed perspiration analysis. (a) Photograph of a wearable FISA on subject's wrist, integrating a multiplexed sweat sensor array and wireless flexible printed circuit board (FPCD) antenna. (b) Photograph of a sensor matrix and circuit for simultaneous and selective measurements of sweat components. Red dashed box indicates location of sensor array and white dashed boxes indicate locations of integrated circuit components. (c) Schematic of sensor array (including glucose, lactate, sodium, potassium, and temperature sensors) for multiplexed perspiration analysis. (d) System-level block diagram of FISA showing signal transduction (orange) (with potential V, current I, and resistance R outputs), conditioning (green), processing (purple), and wireless transmission (blue) paths from sensors to a custom-developed mobile application (numbers in parentheses indicate corresponding labeled components in b); ADC — analogue-to-digital converter. Inset images show home page (left) and real-time data display page (right) of the mobile application. (d) Reproducibility of data for eight glucose sensors. (e) Schematic illustration showing outdoor running group trial based on wearable FISAs (packaged as 'smart headbands'). Data are transmitted to user's cell phone and uploaded to cloud servers [93].

electrode surface was designed to enable precise *in situ* glucose measurement. The fabrication of a biomicrofluidic device, including the formation of flexible electrodes, nanomaterial modification, and enzyme immobilization, was fully realized by inkjet printing to enable simple and low-cost production. As can be seen from Fig. 17b, the use of graphene and platinum nanoparticles significantly enhanced sensor sensitivity. Measurements of H_2O_2 solutions using sensors demonstrated linear dependences of the current on the concentration of peroxide in the solution. Next, layers of Prussian blue and GOx were also printed on the surface of the electrode for glucose analysis. As shown in Fig. 17, the linear range of glucose measurements obtained with the fabricated sensor is from 0 to 400 mg dl^{-1} (0–22 mM), and the detection limit is 0.52 mg dl^{-1} (0.03 mM). The selectivity of the sensor was assessed by adding different substances (dopamine, ascorbic acid, and uric acid) to the glucose solution, which hardly changed the current value. Heating from 20°C to 37°C increased the sensor current by approximately 2.5 times and reduced the time of a single measurement.

Chang et al. [97] demonstrated a highly integrated watch for noninvasive continuous glucose monitoring. The watch employs a Nafion-coated flexible electrochemical patch fixed on a watchband, as shown in Fig. 18. Glucose molecules are detected by two sensors, eliciting a current response that is converted to a voltage signal, amplified, processed, and transmitted to an LED screen. The testing method is simple, making continuous blood glucose monitoring practical and painless. All electronic modules, including a rechargeable power supply and other modules for signal processing and wireless transmission, are integrated onto a watch-face-sized printed circuit board. Blood glucose levels are displayed in real time on the LED screen of the watch and can also be checked using a smartphone user interface.

Chitosan-based composites are believed to have superior mechanical strength, good biocompatibility and biodegradability, remarkable electronic properties, and promising synergistic properties, which greatly enhance their potential for biological applications such as disease diagnosis, biomarker discovery, and drug delivery [98–100]. Biosensors composed of ultrathin single-walled carbon nanotubes and chitosan have demonstrated improved performance in *in situ* sweat analysis [49]. Wang et al. [101] used chitosan modified with reduced graphene oxide (CS@rGO) as a chemiresistor sensor to detect diabetes-related acetone vapors. The authors showed the sensor's high sensitivity even with significant

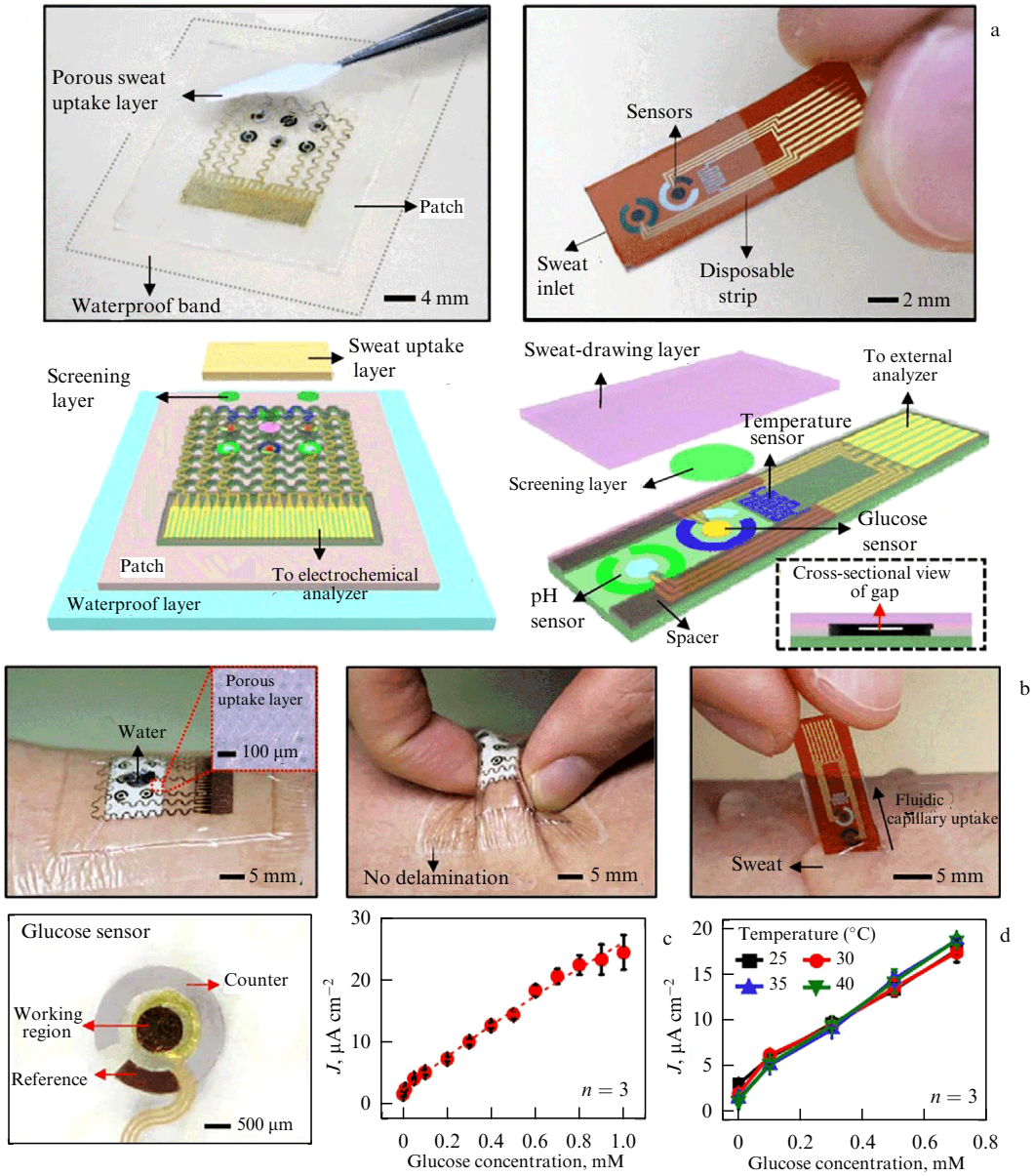

Figure 16. Two variants of disposable sweat and glucose monitoring sensors on different substrates for monitoring sweat and detecting glucose concentration. (a) Optical camera images and (bottom) schematic of wearable sweat monitoring patch. A porous sweat-uptake layer is placed on a Nafion layer and sensors. (b) Optical image of wearable sweat analysis patch under deformation. Inset shows enlarged image of porous sweat uptake layer. (c) Enlarged image of glucose sensor and its calibration curve obtained during electrochemical characterization with known concentration. (d) Calibration curves of glucose sensor at different temperatures [47, 95].

bending, which makes it promising for portable, wearable, or even implantable sensors. The structures presented in Fig. 19 showed good sensitivity specifically to acetone.

Since the sensitivity of an electrochemical biosensor depends on catalytic activity, two-dimensional graphene-like nanomaterials and functionalized graphene are currently the best choice for the latest generation of highly sensitive glucose sensors due to their unique electronic properties [102–105]. As the size decreases, atoms at the corners and edges of nanostructures of different shapes and geometries exhibit different catalytic characteristics, depending on the electronic properties of the corresponding crystallographic surfaces [105]. The electrocatalytic activity of nitrogen-doped graphene can be tuned to reduce H_2O_2 and initiate fast forward electron transfer kinetics in GOx, which holds promise for detecting glucose, even at very low concentrations [104–106]. Thus, a nanocomposite film consisting of functionalized graphene with platinum and GOx-chitosan demonstrates a detection limit of ~ 0.6 μM of glucose [107]. Various biosensors based on nanomaterials such as carbon nanotubes, graphene, and nanofibers have also been implemented for glucose sensing applications [108–114].

Shavelkina et al. [115] and Antonova et al. [116] reported the use of a graphene composite with PEDOT:PSS and ethylene glycol in 2D printing technology for fabricating an inkjet-printed flexible sensor using ordinary office paper. The high conductivity of the composite made it possible to use a thin (approximately 10 nm) layer, the resistance of which can decrease by up to 6 orders of magnitude when the sensor is worn on the skin (Fig. 20). The time needed for a significant change in current when the sensor was worn on the skin was estimated (Fig. 20c). After removing the sensor from the skin,

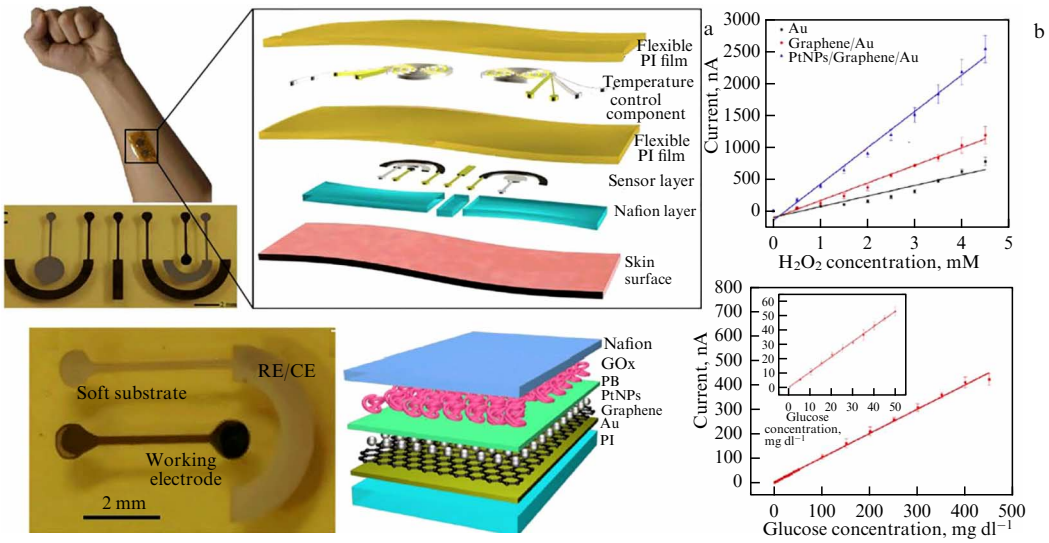

Figure 17. Design of flexible epidermal biomicrofluidic device for continuous blood glucose monitoring. (a) Photo and detailed structure of proposed device. PI film — polyimide film, RE/CE — reference electrode/counter electrode, PB — Prussian blue, and PtNPs — platinum nanoparticles. (b) Amperometric responses and peroxide concentration dependences for different modifications of gold electrode using graphene and Pt nanoparticles. Glucose was monitored after GOx was applied onto the graphene- and Pt nanoparticle-modified electrode [96].

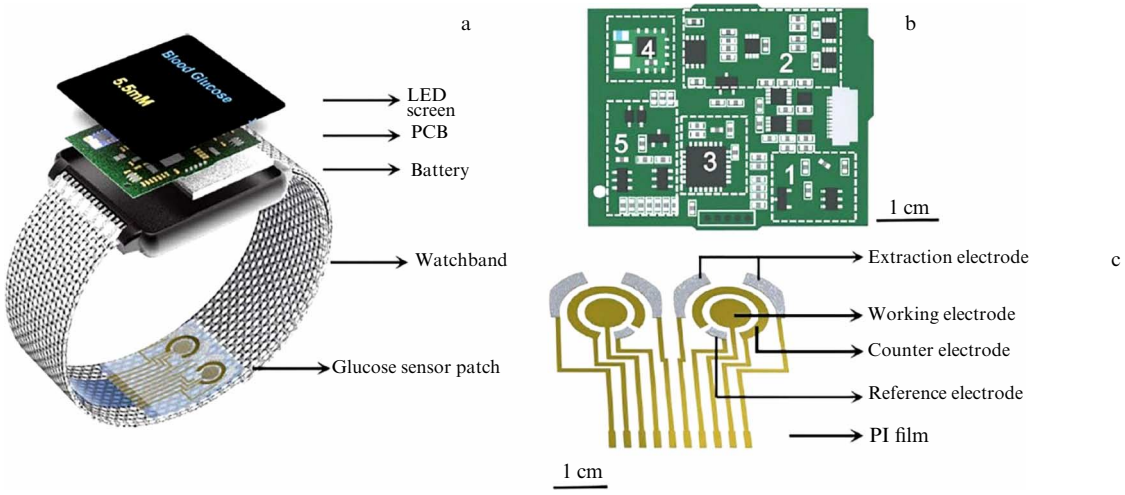

Figure 18. (a) Overall design of a watch for noninvasive continual glucose monitoring. (b) Diagram of printed circuit board (PCB) in the watch showing each functional module: 1 — constant current source, 2 — A/D differential module, 3 — microcontroller, 4 — bluetooth module, and 5 — power supply. (c) Structure of flexible glucose sensor patch for sweat (interstitial fluid) analysis; PI — polyimide film [97].

the signal began to decrease and return to the initial (zero) value 5 to 15 min later (Fig. 20b). The sensor was calibrated for a specific subject, and it or other sensors with the same active layer thickness could be used to measure the glucose level of that subject (Fig. 20d). The response of the sensor was tested after its removal from the hand by measuring its resistance. It should be noted that the sensor made use of thin (thickness from a monolayer to 5 layers) graphene particles synthesized in plasma. In general, this sensor differs from many others in its simplicity of design, the low cost of its fabrication, and the option of reusing the same sensor. An increase in the thickness of the working layer of the sensor leads to a sharp decrease in the sensitivity and selectivity of the sensor.

Panigrahi et al. [107] theoretically examined the potential of a porous nitrogenated graphene (C_2N) monolayer-based glucose sensor to detect glucose molecules by employing van der Waals interactions (Fig. 21). The binding energy turned out to be quite high: −0.93 (−1.31) eV for glucose in the gas phase (aqueous medium); i.e., adsorption of molecules is enhanced in an aqueous environment. The analysis showed that glucose binds to graphene through physisorption and the C_2N monolayer transfers charge to the glucose molecules. Adsorption of glucose molecules on a C_2N monolayer increases the work function compared to pristine C_2N (3.54 eV) by approximately 2.00 eV. Overall, the distinctive properties of graphene-based nanostructures and nitrogenated graphene can be indexed as promising identifiers for glucose sensors using novel nonenzymatic materials for noninvasive blood sugar diagnostics.

Sempionatto et al. [114] presented the first example of a fully integrated eyeglass-based wireless multiplex chemical sensing platform capable of real-time monitoring of sweat components. A new wearable eyeglass-based platform of chemical sensors was realized by integrating potentiometric and amperometric sensors onto the nose bridge pads of the

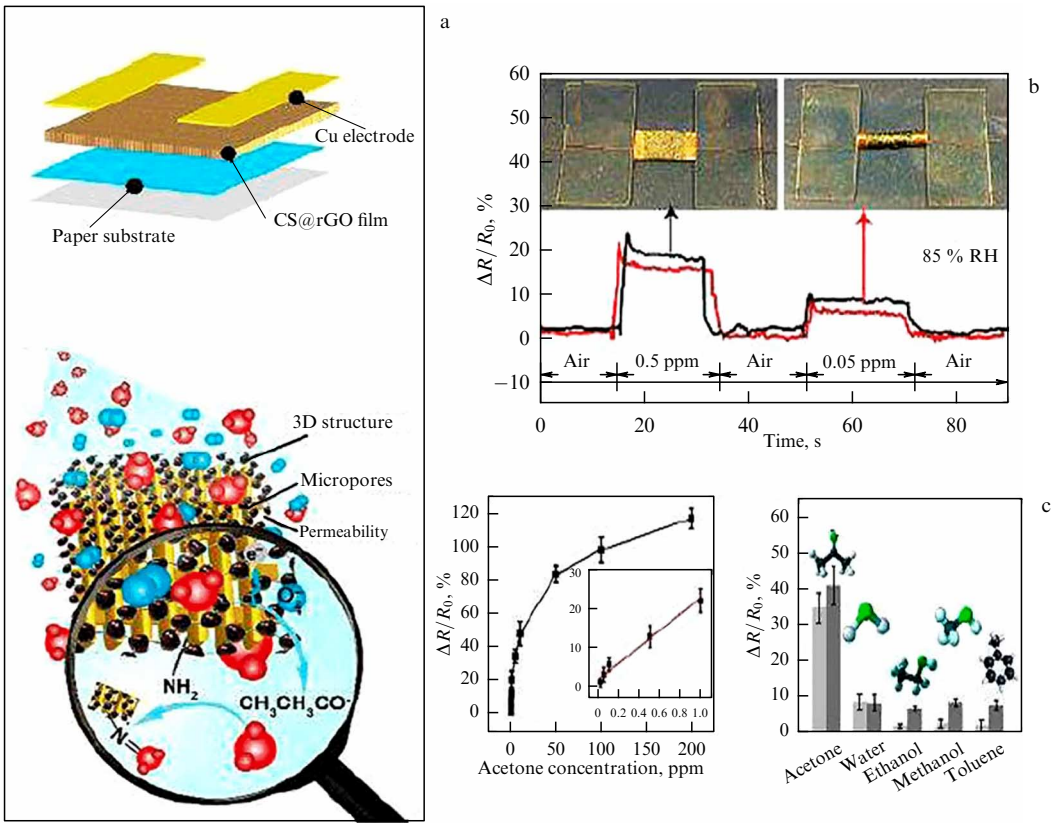

Figure 19. Design, sensing principle, and performance of flexible sensor based on CS@rGO biocomposites. (a) Compositional layout of a single sensor unit, consisting of a CS@rGO biocomposite layer, two copper electrodes, and cellulose paper, as well as resistance measurement principle of an acetone vapor sensor. (b) Comparison of the sensing performance of 3D CS@rGO sensor under flat and bent state. (c) Sensitivity of the sensor as a function of acetone concentration at room temperature and its response values to different types of vapor molecules introduced at a concentration of 5 ppm. Sensor performance evaluated in atmospheric air (light gray) and simulated exhaled breath (dark gray) [101].

glasses and interfacing them to a wireless electronic backbone placed on the temples of the glasses (Fig. 22b). This fully integrated wireless multiplex 'lab on glass' biosensing platform can be easily expanded to simultaneously monitor a large number of sweat components. These electrochemical sensors were screen printed using custom-designed stencils. The three-electrode sensor patterns and contacts were printed on a polyethylene terephthalate (PET) substrate, used as a replacement sticker on the nose pad via double-sided adhesive tape, as shown in Fig. 22a. These easy-to-remove sensor stickers allow the user to select the target for monitoring. Electrochemical nasal pad sensors with a schematic of a potassium sensor (left) and a lactate or glucose sensor (right) are shown in Fig. 22c. Electronic circuitry on the temples of the glasses controls the amperometric and potentiometric transducers and enables wireless data transfer via Bluetooth to the host device. In this way, the lab-on-glass platform can be customized to suit the specific needs of a user.

6. Smart contact lenses for glucose monitoring

Recently, glucose levels in tears have attracted much attention in wearable point-of-care glucose sensors [118–121]. It has been confirmed that the glucose concentration in tears correlates with blood glucose levels [122]. In addition, wearing contact lenses is currently one of the most popular methods of vision correction. As a result, smart contact lenses capable of collecting tears and monitoring the glucose level in tears have become a sought-after wearable device [123–125]. Ruan et al. [125] reported the fabrication of a gelated colloidal crystal attached lens for monitoring tear glucose. This new glucose-responsive sensor consisted of a crystalline colloidal array (CCA) embedded in hydrogel matrix, attached onto a rigid gas permeable (RGP) contact lens. Alternations of the tear glucose concentration between 0 and 50 mM resulted in diffraction of visible light by the sensing contact lens and a wavelength shift from 567 to 468 nm, respectively, thereby leading to a visible color change from reddish yellow to blue. This new point-of-care sensor demonstrated a low detection limit of 0.05 mM, and its combination with a contact lens endowed it with excellent portability and biocompatibility.

Guo et al. [126] developed a multifunctional smart contact lens based on MoS_2 transistors. The PDMS lens substrate contained an MoS_2 transistor-based serpentine mesh glucose sensor for monitoring glucose levels directly from the tear fluid, a photodetector for receiving optical information, and an Au-based temperature sensor for diagnosing potential corneal diseases. This serpentine mesh structure allowed the sensor to maintain direct contact with tears and be mounted directly onto the contact lenses, making it highly sensitive while not interfering with blinking. Moreover, tests revealed the successful biocompatibility of the lens, thus making it promising as a next-generation soft wearable device.

Keum et al. [127] demonstrated a smart contact lens device built on a polymer with excellent biocompatibility. This point-of-care device contained ultra-thin flexible

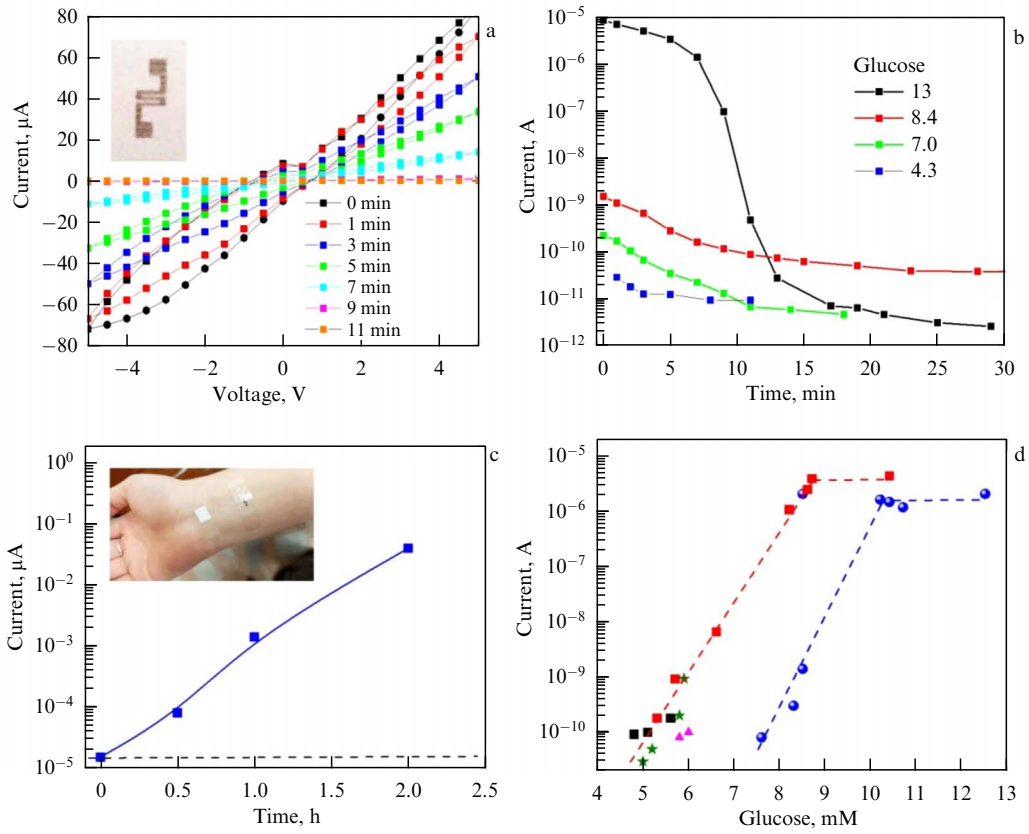

Figure 20. (a) Current–voltage characteristics of wrist-mounted sensor after wearing for 1 h. Inset shows sensor printed on paper and used in this study. (b) Current at 0.5 V as a function of time after removing sensor from the hand for conditions with different values of blood glucose. Glucose values are given as a parameter. (c) Current at 0.5 V as a function of the time sensor is worn on the wrist. Inset shows sensor fixed on the wrist. (d) Current at 0.5 V as a function of values of blood glucose. Different points correspond to different people. Two curves are for healthy people (red) and diabetics (blue) [116].

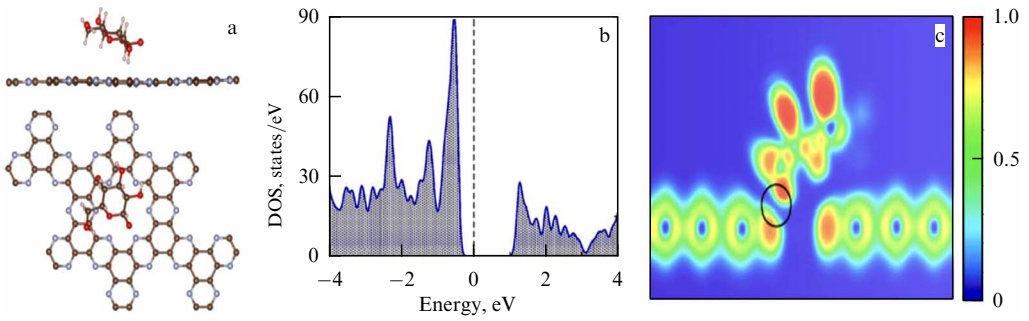

Figure 21. (a) Top view and side view of optimized structure and (b) corresponding density of states (DOS) distribution of C_2N monolayer with an adsorbed glucose molecule. (c) Result of the interaction and two-dimensional electron localization function (ELF) distribution in the cross section of C_2N–glucose structure. ELF values of 0, 0.5, and 1 are interpreted as absence, homogeneous electron gas, and localized electrons, respectively [107].

electronic circuits and a microcontroller chip for tear glucose sensing, drug delivery, data communication, and wireless power management. Contact lens-detected glucose concentrations in tears were shown to correlate with blood glucose levels, allowing the drug delivery to treat diabetic complications. This work pioneered the development of contact lenses capable of biometric analysis in combination with drug delivery, paving the way for personal point-of-care devices and devices with a simultaneous combination of diagnostics and subsequent therapy.

The sensor must be highly permeable to oxygen and water to be compatible with wearable soft contact lenses. Additionally, since wiring the device is impractical, both powering and communication of the sensor response must be done wirelessly. Figure 23a [128] shows a schematic of a device on a soft contact lens in which graphene–silver nanowire (AgNW) composite electrodes and a graphene channel are lithographically deposited on an ultrathin parylene substrate (~500 nm thick). Parylene was chosen as a substrate over other plastic materials due to its intraocular biocompatibility and mechanical superiority such as strength and stretchability. Also, its high transparency and pinhole-free conformal deposition make it a suitable substrate for electrical components of the contact lens.

All components of the device are transparent, with a barely visible spiral antenna, and conformally wrap the

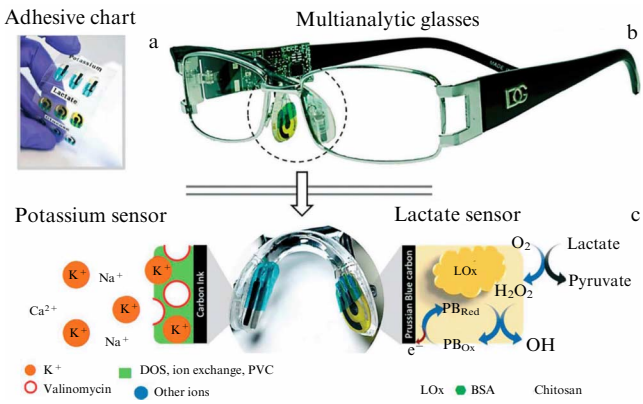

Figure 22. (a) Photograph of interchangeable sticker printed sensors. (b) Photograph of eyeglass biosensor system integrated with wireless circuit board along the temples. (c) Nose pad electrochemical sensors with a schematic of a potassium sensor (left) and a lactate or glucose sensor (right), along with corresponding recognition of metabolites [114]. BSA — bovine serum albumin and LOx — lactate oxidase.

curved surface of the contact lens (radius of curvature, ~1.4 cm; lens thickness, ~0.85 mm). The sensor can be modeled as an electrical resonant RLC circuit, comprising the resistance (R) of the graphene channel, the inductance (L) of the antenna coil made of a graphene–AgNW hybrid material, and the capacitance (C) of source/drain graphene–AgNW electrodes. Wireless operation can be achieved by mutually coupling the sensor with an external antenna, as shown in Fig. 23b. These circuits are connected via an electromagnetic field, which can be characterized by a coupling coefficient [129, 130]. At varied glucose concentrations, a reflection value S_{11} of the wireless sensor was measured at a resonant frequency of 4.1 GHz (Fig. 23c). The reflection increased at higher glucose concentrations, caused by reduced resistance of graphene upon glucose binding. The sensor responds specifically to glucose, even in the presence of interfering substances (50 mM of ascorbic acid, 10 mM of lactate, and 10 mM of uric acid) in the tears. Figure 23d shows a live rabbit with a contact lens sensor for *in vivo* recording. For the *in vivo* test, a contact lens was placed in the rabbit's eye; the rabbit was given about 3 hours to recover from stress and then fed. Taking into account the delayed increase in blood glucose after the food intake, the reflection (S_{11}) was measured after 5 h of the rabbit wearing the lens, or ~ 2 h after feeding. The rabbit showed no signs of abnormal behavior and the sensor remained stable during repeated eye-blinks. After 5 h, the contact lens sensor determined the rabbit's glucose concentration; the data from the sensor were obtained wirelessly while the rabbit was wearing the lens. As shown in Fig. 21e, the contact lens device still functioned and exhibited higher reflection than the value before wearing, presumably due to glucose binding. The sensing platform integrated onto the contact lens enables wireless and real-time monitoring of tear glucose levels and does not require finger pricking [128].

Another option for a contact lens is shown in Fig. 24 [124]. A rectifier, LED, glucose sensor, and antenna are the circuit elements on the contact lens. Glucose oxidase is immobilized on the surface of the graphene channel. The smart contact lens wirelessly transfers electrical power to the lens through the antenna, which activates the LED and the glucose sensor. The LED (indicator) turns off once the detected glucose level exceeds the normal limit. The signal receiver is placed at a distance of 10 mm from the contact lens to collect the signal from the antenna. An RF transmitter and a thin-film rechargeable battery are integrated with the contact lens. The system was tested *in vitro* to detect glucose levels in the range of 3–25 mg dl^{-1} (0.17–1.4 mM) and showed a linear response.

The most significant challenge for tear glucose sensors is the power supply. Because the human eye is sensitive, the power supply must be weak, and the external power supply

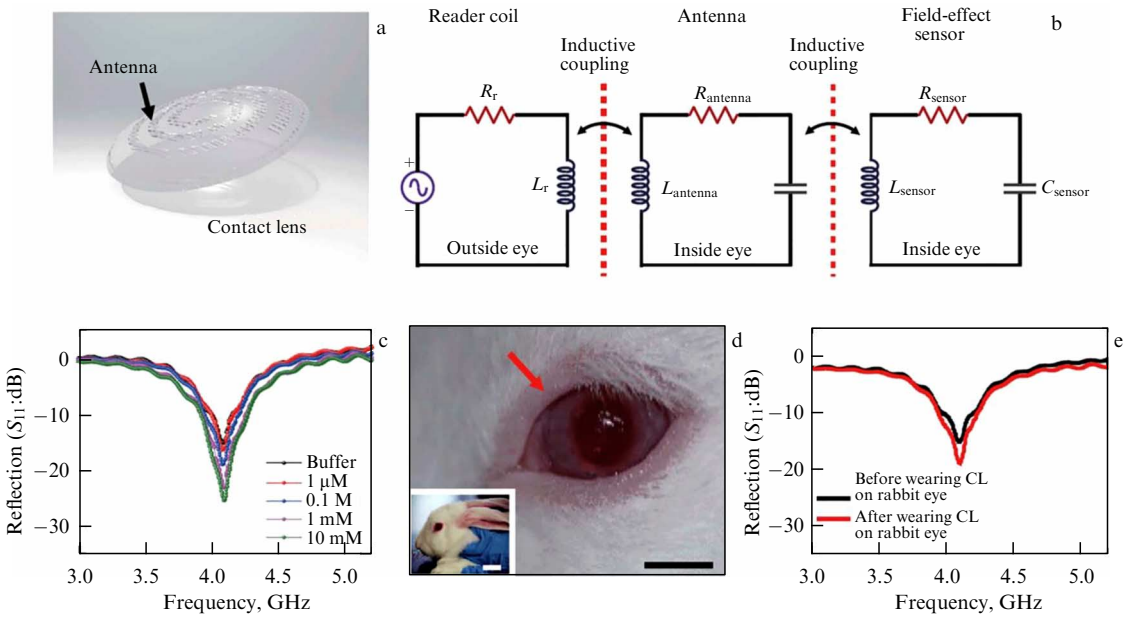

Figure 23. Contact lens sensor for wireless detection of glucose. (a) Schematic illustration of transparent glucose sensor on a contact lens. (b) Schematic of reading circuit for wireless sensing on the contact lens. (c) Wireless monitoring of glucose concentrations from 1 mM to 10 mM. (d) Photographs of wireless sensor integrated onto the eyes of a live rabbit. Black and white scale bars, 1 cm and 5 cm, respectively. (e) Wireless sensing curves of glucose concentration before and after wearing the contact lens on the eye of a live rabbit [128]; CL — contact lens.

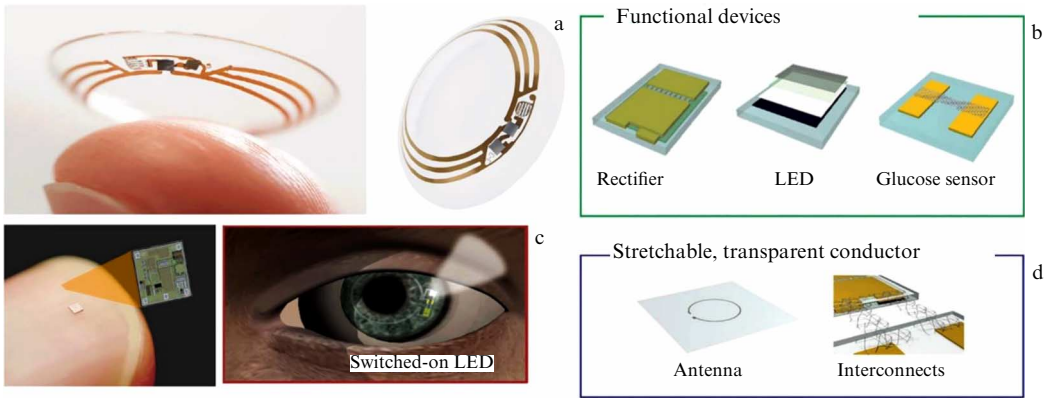

Figure 24. (a) External appearance and (b, d) schematic illustration of soft, smart contact lens: lens is composed of (b) a hybrid substrate, functional devices (rectifier, LED, and glucose sensor), and (d) a transparent stretchable conductor (for antenna and interconnects). (c) Printed circuit board and operation of the smart contact lens system [124].

used in most scientific research nowadays will cause a great deal of discomfort to the user.

7. Comparative analysis of the wearable sensor responses

One of the important parameters of wearable sensors is their sensitivity, defined as the current generated in the sensor device normalized to the sensor area and glucose being detected. The table shows the sensitivity for a number of sensors using carbon materials (graphene, reduced graphene oxide, carbon nanotubes, and carbon nano-onions) [132–145]. The electrochemical sensitivity of common materials used for wearable sensors is usually determined in solutions with a known glucose concentration, i.e., at the initial stage of development of a wearable sensor. One can see from the table that the sensitivity varies widely depending on the specific design of the working electrode. Thus, a fairly high sensitivity value of the ZnO/CNO electrode is associated with the oxidation of glucose on the electrode due to the high catalytic activity of ZnO and the high electrical conductivity of carbon nano-onions (CNOs) [133]. The use of weakly conductive graphene oxide in [142, 143] led to low sensitivity of the electrode, despite the presence of ZnO and GOx in it.

High sensitivity was obtained to develop a nonenzymatic glucose sensor with an active nitrogen-doped CuO/carbon nanotube (CuO–CN) layer [145]. Chitosan was used to prepare a nanostructured carbon material doped with nitrogen, and the method for its preparation is described in more detail in [146]. A possible mechanism of direct electrochemical

Table. Comparison of sensitivity and range of linear dependence of a signal on glucose concentration and other parameters of wearable carbon-based sensors.

Active layer of the sensor	Sensitivity, $\mu A\ mM^{-1}\ cm^{-2}$	Linear range, mM	Potential, V	Ref.
NiO–CuO/CFME (graphene fibers)	70	0.001–0.57	0.6	[131]
CuO/CN	1546	0.05–1.0	0.6	[132]
ZnO/CNO	606	0.1–15	1.5	[133]
CuNPs/rGO/SPCE	172	0.10–12.5	0.8	[134]
SWCNTs/Cu_2O/ZnO NPs/G	466	0.6–11.1	0.8	[135]
NH_2 – G/$Cu_3(btc)_2$NP	5.4	0.05 ~ 1.8	0.8	[136]
Pt:G/hydrogel/GOx	37	0.006–0.7	0.4	[137]
N–G airgel–CuO	223	0.01–6.7	0.4	[138]
GOx/ZnO/Cu_2O/GO	0.06	0.01–2	0.8	[139]
Cu_2O/rGO	285	0.3–3.3	0.8	[140]
CuNPs/G	607	0.005–1.4	0.5	[141]
CuO NP/G	1360	0.002–4	0.6	[142]
GOx/ZnO/GO	19	0.02–6.2	0.8	[143]
PtAuNP/ rGO/GOx	48	0.001–2.4	0.4–0.7	[144]
MWCNT – Au@NiO@CuO	1637	0.001–5.6	0.4	[145]
CFME — Carbon Fiber MicroElectrode, CN — nitrogen-doped carbon nanocomposite, CNO — Carbon Nano-Onion, SPCE – Screen-Printed Carbon Electrode, and NP — nanoparticle.				

oxidation of glucose can be described by the reactions

$$\begin{aligned} &\mathrm{Cu(II)} = \mathrm{Cu(III)} + \mathrm{e}^- \\ &\mathrm{Cu(III)} + \text{glucose} = \mathrm{Cu(II)} + \text{gluconolactone} \\ &\text{gluconolactone} \rightarrow \text{gluconic acid}\,. \end{aligned} \qquad (2)$$

Initially, Cu(II) electrochemically oxidizes to Cu(III). The reaction between Cu(III) and glucose leads to the oxidation of glucose to gluconolactone, and Cu(III) is reduced to Cu(II). Finally, gluconolactone is converted to gluconic acid through hydrolysis. This mechanism is typical of the indirect oxidation of glucose not only with the participation of copper but also with other metals (Pt, Au, ZnO, etc.) and nanostructured carbon (graphene, carbon tubes, etc.), as described previously, for example, in [142, 147, 148]. In addition, carbon materials, having good conductivity, ensure a quick response of the sensor to changes in the glucose level. A successful combination of components led to a high sensitivity of sensors (see Refs [135, 141, 142, 145]).

8. Long-term glucose monitoring

A graphene fiber fabric assembled by wet-fused graphene fibers provides superior electrical performance and mechanical properties, as well as fluid permeation paths, demonstrating great potential for electrochemical glucose monitoring (Fig. 25) [149]. This fabric as a sensor patch ensures good air permeability, which is necessary for comfortable, long-term wearing of the sensor but has rarely been addressed. Graphene decorated with Prussian blue exhibits a high electrochemical sensitivity to hydrogen peroxide (7298 μA $\mathrm{mM^{-1}\ cm^{-2}}$). After being modified by glucose oxidase and chitosan, it provides high selectivity, but lower electrochemical sensitivity to glucose (1540 μA $\mathrm{mM^{-1}\ cm^{-2}}$ in the sweat glucose concentration range of 2–220 μM and 948 μA $\mathrm{mM^{-1}\ cm^{-2}}$ in the concentration range of 220–650 μM). High sensitivity is most likely due to the relatively high conductivity (electron mobility) in the working layer of the sensor.

The low density of electrochemically active defects in graphene synthesized by chemical vapor deposition limits its use in biosensors. However, graphene doped with gold and combined with a gold mesh has improved electrochemical activity compared to pristine graphene, sufficient to form a sensor for sweat-based glucose monitoring (Fig. 26) [150]. The stretchable device features a serpentine bilayer of gold mesh and gold-doped graphene, forming an efficient electrochemical interface for stable transmission of electrical signals. The patch consists of a heater; temperature, humidity, glucose, and pH sensors; and polymer microneedles that can be thermally activated to deliver drugs.

Oh et al. [151] used layer-by-layer deposition of carbon nanotubes (CNTs) on top of patterned Au nanosheets (AuNSs) prepared by filtration onto stretchable substrates to fabricate a sensor electrode. For glucose detection and pH measurement, CoW_4/CNT and polyaniline/CNT composites, respectively, were further coated onto the CNT-AuNS electrodes. The sensor demonstrated a high sensitivity of 10.9 μA $\mathrm{mM^{-1}\ cm^{-2}}$ for glucose, with mechanical stability of up to 30% stretching and temporal stability for 10 days (Fig. 27).

Zhu et al. [152] reported highly sensitive and reproducible long-term continuous nonenzymatic glucose monitoring *in vivo*. The process is based on the electrocatalytic reaction of

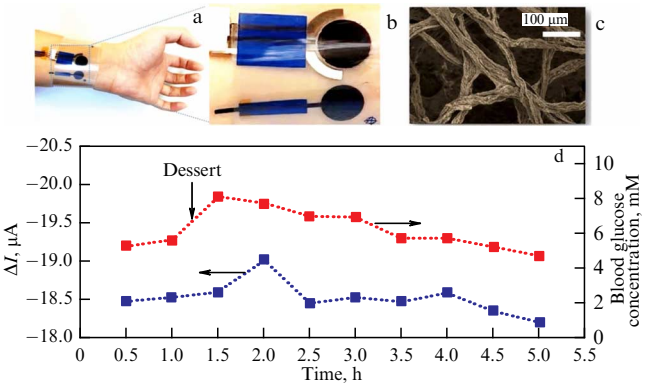

Figure 25. (a) Images of a sensing patch on a volunteer's wrist and (b) enlarged view of the sensor and iontophoretic anode. (c) SEM image of sensing graphene oxide fiber fabric. (d) Results of glucose monitoring in 5-h period by using a finger-prick glucometer (red) and the sensing patch (blue) [149].

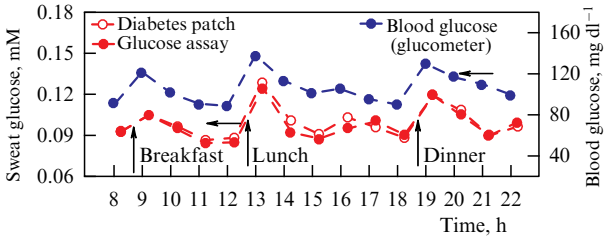

Figure 26. One-day monitoring of glucose concentrations in sweat and blood of a human [150].

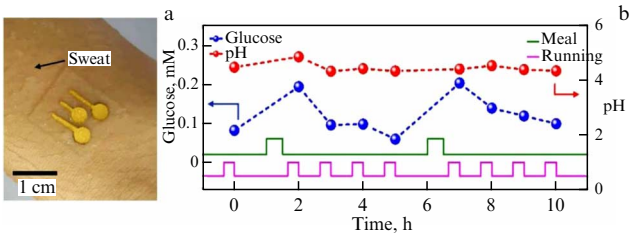

Figure 27. (a) Photo of electrochemical sensor attached to the skin. (b) Change in glucose concentration and pH measured by sensor attached to skin along with different activities of meal intake (green line) and running (purple line) for 10 h. All data were calibrated with temperature-dependent sensitivity at 30 °C [151].

water splitting in the presence of Pd nanoparticles encapsulated in a cobalt-based zeolite imidazolate framework [Co(Pd@ZIF-67)]. Carbon paste with Pd@ZIF-67 is prepared and screen-printed onto a flexible PET substrate as the working electrode. A multistage potential is applied to the electrode, including a high negative potential for pretreatment, which produces a local alkaline condition through a water splitting reaction. The high negative potential step results in the production of the hydroxyde ion from water on the surface of the working electrode via the reaction

$$2\mathrm{H_2O} + 2\mathrm{e} \xrightarrow{-2.0\,\mathrm{B}} \mathrm{H_2} + 2\mathrm{OH}\,. \qquad (3)$$

Note that Pd nanoparticles encapsulated in the metal–organic framework $[\mathrm{Co(mim)_2(OH)}]_n$ serve to prevent the formation of hydrogen bubbles in order to ensure the accuracy of the subsequent quantitative assay of glucose due to reactions similar to reactions (2) by converting $[\mathrm{Co(III)(mim)_2(OH)}]_n$ to $[\mathrm{Co(IV)(mim)_2(OH)}]_n$, followed by

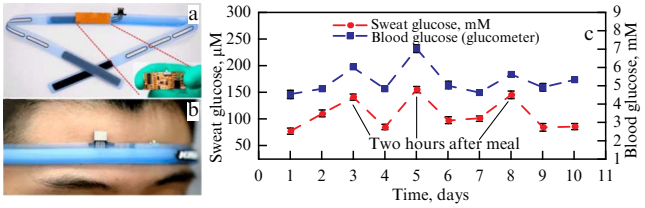

Figure 28. (a) Photograph of Pd@ZIF-67-based nonenzymatic glucose sensor system integrated into a sweatband. (b) Photograph of the sensing system on the sweatband. (c) Monitoring of glucose concentration in sweat and blood of a human within 10 days. Error bars represent standard deviations for three replicated measurements [152].

oxidation of glucose. Finally, a positive potential is applied to clean and regenerate the electrode for the next assay. A fully integrated sweatband with a sensor is designed for real-time analysis of sweat glucose during physical exercise. The long-term stability and robustness of the sensor are also evaluated.

A sensing system comprising an electrochemical sensor and a flexible printed circuit board (FPCB) with Bluetooth connectivity to an Android-based smartphone application was fabricated and integrated into a sweatband for wearable sensing (Fig. 28). Before on-body tests, the sensor was calibrated using liquid chromatography. Volunteers testing the sensors in the laboratory were asked to wear the sweatband and ride a bicycle, and after a testing time (Fig. 28), the result was displayed on the smartphone screen. Monitoring data for sweat and blood glucose levels over 10 days are presented in Fig. 28c (blood glucose was measured using a glucometer). Tests on days 3, 5, and 8 were intentionally performed 2 h after meals. Sweat glucose concentration (left y-axis) obtained using the developed sensor correlated well with blood glucose concentration (right y-axis). For the case of physical activity, the coefficient, which is the ratio of the concentration of glucose in sweat to the concentration of glucose in the blood, is about 0.2. In addition, glucose in the sweat sample was analyzed using chromatography. The average relative error was 19.7%.

An interesting version of a continuous sweat sensor was proposed by Daboss et al. [153], who used nanoparticles with a diameter of ~ 50 nm with a Prussian blue core (35–37 nm) and a shell of nickel hexacyanoferrate nanoferrates. The shell was designed to stabilize particles and increase the service life of Prussian blue nanoparticles as a catalyst for the reaction with hydrogen peroxide. The authors showed that the sensitivity of the sensor decreases with increasing nanoparticle size. This sensor was a flow-through multibiosensor (similar to that in [77]) for the simultaneous assay of glucose and lactate, which allows hypoxia and glycemia to be noninvasively continuously monitored.

9. Conclusions and development prospects

We have discussed the main approaches and the most interesting examples from a wide range of proposed wearable sensors developed in the last decade. Note that many different sensors are being developed, each having its own advantages and disadvantages. The emergence of new and the development of existing noninvasive sensors will depend on advances in simple, inexpensive, and effective sensors and their integration with transmitting and receiving electronics, allowing medical point-of-care devices to be tailored to an individual patient's requirements.

The most advanced sensors are based on the enzyme glucose oxidase or its analogues. However, such structures are more complex (consisting of several layers, including a porous protective layer), require stimulation of sweat excretion, are more expensive and, as a rule, are disposable. Enzymes can be replaced by metal nanoparticles, but their use has not yet been sufficiently developed. Sensors based on patterned carbon materials (graphene, carbon quantum dots, carbon tubes, and nano-onions) often excel at providing a good response, but at the same time they are much less studied. As with fermented electrodes, glucose is assumed to oxidize, although this issue requires further research.

While throughout the world there are a plethora of research groups involved in the development of noninvasive glucose sensors, they are few in number in Russia. A group under the leadership of A A Karyakin (see papers [77, 153]) from Lomonosov Moscow State University has been working on this topic for a long time. Recently, a group headed by I V Antonova (see papers [115, 116]) from the Rzhanov Institute of Semiconductor Physics, Siberian Branch of the Russian Academy of Sciences (Novosibirsk) has joined the efforts in this field.

In general, the prospect of designing noninvasive glucose sensors is extremely in demand in modern society. It is especially important that such systems be reliable, simple, and cheap, i.e., available for daily at-home glucose monitoring. Currently, other versions of noninvasive sensors in the form of 'watches' already exist, and are expected to appear on the market (see Fig. 18 and, for example, [97]). It is worth noting that currently available smartwatch glucometers cannot be used for medical purposes, as the measurement of blood glucose levels have not been proven to be accurate, especially levels higher than 9, as indicated in the user's manual for the GLE-04 watch model. Then there is the issue of the cost of the sensors. The development of cheap sensors remains extremely relevant. Moreover, it is necessary to distinguish between household glucose sensors, for which the most important parameters are accessibility (low cost) and simplicity, and medical sensors, when accuracy and reliability come to the fore.

References

1. International Diabetes Federation, IDF Diabetes Atlas, 10th ed., Brussels, Belgium. 2021, accessed 28.03.2023, https://www.diabetesatlas.org
2. Hatada M et al. *Sens. Actuators B* **351** 130914 (2022)
3. Liu J, Bao S, Wang X *Micromachines* **13** 184 (2022)
4. Pullano S A et al. *Theranostics* **12** 493 (2022)
5. Chen Z et al. *Green Chem.* **26** 3801 (2024)
6. Clark L C (Jr.), Lyons C *Ann. New York Acad. Sci.* **102** 29 (1962)
7. Updike S J, Hicks G P *Nature* **214** 986 (1967)
8. Guilbault G G, Lubrano G J *Anal. Chim. Acta* **64** 439 (1973)
9. Tarasov Yu V et al. *Problemy Endokrinologii* **61** (4) 54 (2015) https://doi.org/10.14341/probl201561454-72
10. Wang J *Electroanalysis* **13** 983 (2001)
11. Rahman M M et al. *Sensors* **10** 4855 (2010)
12. Sabu C et al. *Biosens. Bioelectron.* **141** 111201 (2019)
13. Niu X H et al. *Anal. Methods* **8** 1755 (2016)
14. Pu Z et al. *Biomicrofluidics* **10** 011910 (2016)
15. Peña-Bahamonde J et al. *J. Nanobiotechnol.* **16** 75 (2018)
16. Ferreira R G, Silva A P, Nunes-Pereira J *ACS Sens.* **9** 1104 (2024)
17. Peng B et al. *Small* **16** 2002681 (2020)
18. Jang M et al. *Sensors* **22** 6985 (2022)
19. Khoshmanesh F et al. *Biosens. Bioelectron.* **176** 112946 (2021)
20. Wei S et al. *J. Mater. Sci. Technol.* **37** 71 (2020)
21. Liu Y et al. *RSC Adv.* **6** 18654 (2016)
22. Gao W, Brooks G A, Klonoff D C *J. Appl. Physiol.* **124** 548 (2018)

23. Dang W et al. *Biosens. Bioelectron.* **107** 192 (2018)
24. Alizadeh N, Salimi A, Hallaj R *Microchim. Acta* **187** 14 (2020)
25. Qu Z et al. *Chem. Commun.* **49** 9830 (2013)
26. Tuchin V V (Ed.) *Handbook of Optical Sensing of Glucose in Biological Fluids and Tissues* (Boca Raton, FL: CRC Press, 2009)
27. Dunaev A, Tuchin V (Eds) *Biomedical Photonics for Diabetes Research* (Boca Raton, FL: CRC Press, 2022)
28. Yu Z et al. *Prog. Biomed. Eng.* **3** 022004 (2021)
29. Larin K V et al. *Phys. Med. Biol.* **48** 1371 (2003)
30. Chen T-L et al. *J. Biomed. Opt.* **23** 047001 (2018) https://doi.org/10.1117/1.JBO.23.4.047001
31. Phan Q-H, Lo Y-L *Opt. Lasers Eng.* **92** 120 (2017)
32. Othman H O, Hassan R O, Faizullah A T *Microchem. J.* **163** 105919 (2021)
33. Wu W et al. *Angew. Chem. Int. Ed.* **49** 6554 (2010)
34. Sun X *Anal. Chim. Acta* **1206** 339226 (2022)
35. Haynes C L et al. *J. Raman Spectrosc.* **36** 471 (2005)
36. Lyandres O et al. *Diabetes Technol. Therapeut.* **10** 257 (2008)
37. Liu Y et al. *Biosens. Bioelectron.* **94** 131 (2017)
38. Dina N E et al. *Anal. Chem.* **90** 2484 (2018)
39. Bantz K C et al. *Phys. Chem. Chem. Phys.* **13** 11551 (2011)
40. Chen H et al. *ACS Sens.* **6** 2378 (2021)
41. Jin C M, Joo J B, Choi I *Anal. Chem.* **90** 5023 (2018)
42. Perez-Mayen L et al. *Nanoscale* **8** 11862 (2016)
43. Yang D et al. *Anal. Chem.* **90** 14269 (2018)
44. Hu S et al. *ACS Appl. Mater. Interfaces* **12** 55324 (2020)
45. Lyandres O et al. *Analyst* **135** 2111 (2010)
46. Lussier F et al. *ACS Nano* **13** 1403 (2019)
47. He X et al. *Anal. Chem.* **91** 4296 (2019)
48. Koh A et al. *Sci. Transl. Med.* **8** 366ra165 (2016) https://doi.org/10.1126/scitranslmed.aaf2593
49. Xiao J et al. *Anal. Chem.* **91** 14803 (2019)
50. Ray T R et al. *Sci. Transl. Med.* **13** (587) eabd8109 (2016) https://doi.org/10.1126%2Fscitranslmed.abd8109
51. Klasner S A et al. *Anal. Bioanal. Chem.* **397** 1821 (2010)
52. Bandodkar A J et al. *Sci. Adv.* **5** eaav3294 (2019)
53. Han H et al. *ACS Nano* **12** 932 (2018)
54. Hou J et al. *Small* **11** 2738 (2015)
55. Cui Y et al. *ACS Sens.* **5** 2096 (2020)
56. Nyein H Y Y et al. *Sci. Adv.* **5** eaaw9906 (2019)
57. Saha S et al. *Sci. Rep.* **7** 6855 (2017)
58. Hanna J et al. *Sci. Adv.* **6** eaba5320 (2020)
59. Choi H et al., in *Proc. of the 2017 IEEE MTT-S Intern. Microwave Symp., IMS 2017, Honolulu, Hawaii, USA, 4–9 June 2017* (Piscataway, NJ: IEEE, 2017) p. 876
60. Yilmaz T, Foster R, Hao Y *Diagnostics* **9** 6 (2019)
61. Cherevko A G et al. *Materials* **15** 7267 (2022)
62. Zhang J et al. *ACS Omega* **5** 12937 (2020)
63. Omer A E et al. *Sci. Rep.* **10** 15200 (2020)
64. Bariya M, Nyein H Y Y, Javey A *Nat. Electron.* **1** 160 (2018)
65. Mani V et al. *TrAC Trends. Anal. Chem.* **135** 116164 (2021)
66. Ren X et al. *ACS Sens.* **8** 2691 (2023)
67. Sieg A, Guy R H, Delgado-Charro M B *J. Pharma. Sci.* **92** 2295 (2003)
68. Holze R "Book Review: Electrochemical Methods. Fundamentals and Applications (2nd Edition). By Allen J. Bard and Larry R. Faulkner" *Angew. Chem. Int. Ed.* **41** 655 (2002)
69. Zhang S et al. *Front. Bioeng. Biotechnol.* **9** 774210 (2021)
70. Zheng L, Liu Y, Zhang C *Sens. Actuators B* **343** 130131 (2021)
71. Veeralingam S, Khandelwal S, Badhulika S *IEEE Sensors J.* **20** 8437 (2020)
72. Bauer M et al. *Anal. Bioanal. Chem.* **413** 763 (2021)
73. Xiao J et al. *Anal. Chem.* **91** 14803 (2019)
74. Jin X et al. *Biosens. Bioelectron.* **196** 113760 (2022)
75. Heikenfeld J *Electroanalysis* **28** 1242 (2016)
76. Sonner Z et al. *Biomicrofluidics* **9** 031301 (2015)
77. Karpova E V et al. *Anal. Chem.* **91** 3778 (2019)
78. Sabury S, Kazemi S H, Sharif F *Mater. Sci. Eng. C* **49** 297 (2015)
79. Mazaheri M, Simchi A, Aashuri H *Microchim. Acta* **185** 178 (2018)
80. Gutés A, Carraro C, Maboudian R *Biosens. Bioelectron.* **33** 56 (2012)
81. Wu B et al. *Nanomaterials* **8** 993 (2018)
82. Maity D, Minitha C R, Rajendra Kumar R T *Mater. Sci. Eng. C* **105** 110075 (2019)
83. Akhtar M A et al. *ACS Appl. Nano Mater.* **2** 1589 (2019)
84. Yuan Y et al. *J. Electroanal. Chem.* **855** 113495 (2019)
85. Peña-Bahamonde J et al. *J. Nanobiotechnol.* **16** 75 (2018)
86. Zhang Z et al. *Lab Chip* **19** 3448 (2019)
87. Zhang X et al. *Anal. Chem.* **90** 11780 (2018)
88. Sempionatto J R, Moon J-M, Wang J *ACS Sens.* **6** 1875 (2021)
89. Jang H et al. *Nat. Commun.* **13** 6604 (2022)
90. Ameri S K et al. *ACS Nano* **11** 7634 (2017)
91. Bandodkar A J et al. *Biosens. Bioelectron.* **54** 603 (2014)
92. Jia W et al. *Anal. Chem.* **85** 6553 (2013)
93. Gao W et al. *Nature* **529** 509 (2016)
94. He X et al. *npj Flexible Electron.* **6** 60 (2022)
95. Lee H et al. *Sci. Adv.* **3** e1601314 (2017)
96. Pu Z et al. *Sci. Adv.* **7** eabd0199 (2021)
97. Chang T et al. *Microsyst. Nanoeng.* **8** 25 (2022)
98. Gordonov T et al. *Nat. Nanotechnol.* **9** 605 (2014)
99. Zhang M G, Gorski W *J. Am. Chem. Soc.* **127** 2058 (2005)
100. Cuña M et al. *J. Nanosci. Nanotechnol.* **6** 2887 (2006)
101. Wang L et al. *J. Mater. Chem. B* **5** 4019 (2017)
102. Tehrani F, Bavarian B *Sci. Rep.* **6** 27975 (2016)
103. Wang Y et al. *ACS Nano* **4** 1790 (2010)
104. Wang Z et al. *J. Phys. Chem. C* **113** 14071 (2009)
105. Cao S et al. *Chem. Soc. Rev.* **45** 4747 (2016)
106. Haghighi N, Hallaj R, Salimi A *Mater. Sci. Eng. C* **73** 417 (2017)
107. Panigrahi P et al. *Appl. Surf. Sci.* **573** 151579 (2022)
108. Wu H et al. *Talanta* **80** 403 (2009)
109. Taguchi M et al. *J. Diabetes Sci. Technol.* **8** 403 (2014)
110. Hussain T et al. *Carbon* **163** 213 (2020)
111. Emaminejad S et al. *Proc. Natl. Acad. Sci. USA* **114** 4625 (2017)
112. Kinnamon D et al. *Sci. Rep.* **7** 13312 (2017)
113. Imani S et al. *Nat. Commun.* **7** 11650 (2016)
114. Sempionatto J R et al. *Lab Chip* **17** 1834 (2017)
115. Shavelkina M B et al. *High Energy Chem.* **57** (Suppl. 1) S200 (2023)
116. Antonova I V et al. *Phys. Chem. Chem. Phys.* **26** 7844 (2024)
117. Batvani N et al. *Sensing Bio-Sensing Res.* **38** 100532 (2022)
118. Farandos N M et al. *Adv. Healthcare Mater.* **4** 792 (2015)
119. Elsherif M et al. *Front. Med.* **9** 858784 (2022)
120. Lee H et al. *Adv. Healthcare Mater.* **7** 1701150 (2018)
121. Chatterjee P R et al. *J. Indian Med. Assoc.* **101** 481 (2003)
122. Elsherif M et al. *ACS Nano* **12** 5452 (2018)
123. Lin Y-R et al. *Sensors* **18** 3208 (2018)
124. Park J et al. *Sci. Adv.* **4** eaap9841 (2018)
125. Ruan J-L et al. *Polymers* **9** 125 (2017)
126. Guo S et al. *Matter* **4** 969 (2021)
127. Keum D H et al. *Sci. Adv.* **6** eaba3252 (2020)
128. Kim J et al. *Nat. Commun.* **8** 14997 (2017)
129. Mannoor M S et al. *Nat. Commun.* **3** 763 (2012)
130. Na K et al. *IEEE Sens. J.* **16** 5003 (2016)
131. Park J et al. *Nanoscale* **8** 10591 (2016)
132. Figiela M et al. *Electroanalysis* **34** 1725 (2022)
133. Sharma A et al. *ACS Omega* **7** 37748 (2022)
134. Phetsang S et al. *Sci. Rep.* **11** 9302 (2021)
135. Chen H-C, Su W-R, Yeh Y-C *ACS Appl. Mater. Interfaces* **12** 32905 (2020)
136. Wang Z et al. *Nanoscale* **10** 6629 (2018)
137. Lipani L et al. *Nat. Nanotechnol.* **13** 504 (2018)
138. Felix S et al. *Appl. Phys. A* **123** 620 (2017)
139. Elahi M Y, Khodadadi A A, Mortazavi Y *J. Electrochem. Soc.* **161** B81 (2014)
140. Liu M, Liu R, Chen W *Biosens. Bioelectron.* **45** 206 (2013)
141. Luo J et al. *Microchim. Acta* **177** 485 (2012)
142. Luo L, Zhu L, Wang Z *Bioelectrochemistry* **88** 156 (2012)
143. Palanisamy S, Vilian A T E, Chen S-M *Int. J. Electrochem. Sci.* **7** 2153 (2012)
144. Xuan X, Yoon H S, Park J Y *Biosens. Bioelectron.* **109** 75 (2018)
145. Zhang Q et al. *Appl. Surf. Sci.* **515** 146062 (2020)
146. Figiela M et al. *Sens. Actuators B* **272** 296 (2018)
147. Mathew M, Sandhyarani N *Electrochim. Acta* **108** 274 (2013)
148. Phetsang S et al. *Sci. Rep.* **11** 9302 (2021)
149. Cai S et al. *Nano Energy* **93** 106904 (2022)
150. Lee H et al. *Nat. Nanotechnol.* **11** 566 (2016)
151. Oh S Y et al. *ACS Appl. Mater. Interfaces* **10** 13729 (2018)
152. Zhu X et al. *Anal. Chem.* **91** 10764 (2019)
153. Daboss E V, Shcherbacheva E V, Karyakin A A *Sens. Actuators B* **380** 133337 (2023)